Self-Adaptation of Multi-Recombinant Evolution Strategies on the Highly Multimodal Rastrigin Function

Amir Omeradzic and Hans-Georg Beyer

***Abstract*—The self-adaptive, multi-recombinative $(\mu/\mu_I, \lambda)$-ES (Evolution Strategy) is investigated on the highly multimodal Rastrigin test function by theoretical and experimental means. The analysis is based on the established dynamical systems approach. To this end, the self-adaptation response function is derived in the limit of large populations, which are necessary to achieve high success rates. Furthermore, steady-state conditions on Rastrigin are discussed and compared to the sphere function. Then, a relation for the learning parameter τ is derived to tune the sampling process of the self-adaptive ES, improving its efficiency on Rastrigin. The obtained result is compared to default τ-values. Furthermore, expected runtime experiments are conducted varying τ and population parameters of the ES. Theoretical and experimental results regarding τ are compared in terms of efficiency and robustness showing good agreement.**

***Index Terms*—Evolution Strategy, Rastrigin Function, Self-Adaptation, Multimodality**

I. Introduction

THE optimization of real-valued highly multimodal test functions poses a major challenge for conventional gradient-based optimization algorithms. Evolutionary Algorithms, such as Evolution Strategies (ES) [1], have experimentally proven to be capable of localizing the global optimizer among a vast number of local optima provided that the strategy parameters are chosen appropriately [2]. Besides the population size [3], [4], a key ingredient to improve global search is the adaptation of the mutation strength σ. State-of-the-art implementations for ES are self-adaptation (σSA) [5], [6], [7] and cumulative step-size adaptation (CSA) [8], [9]. CSA works by comparing a measured σ-path-length to the path length expected under random selection. Self-adaptation, which is the focus of this paper, samples offspring mutation strengths from a distribution (usually log-normal). Selection by fitness implicitly selects corresponding mutation strengths. Multimodal functions, among others, have been (and are still) studied empirically using the Black-Box Optimization Benchmarking (BBOB) suite [10]. Exemplary results are given in [11]. The approach aims at comparing a set of optimization algorithms on multiple different problem instances by aggregating the corresponding empirical runtime data. The goal of the present paper is to provide a more detailed analysis of the Rastrigin function using a self-adaptive ES and link theoretical results to empirical data.

Self-adaptive ES have been investigated theoretically on unimodal functions, such as the sphere [7], [12] and the general ellipsoid model [13]. All studies aim at the derivation of recommended parameter settings for the σ-sampling which is controlled by the learning parameter τ. Initially in [14], a scaling law for $\tau(N)$ was derived inversely proportional to the square root of the dimension N. Later, [7] derived an appropriate proportionality constant for the $(1, \lambda)$-ES on the sphere, while [12] derived the corresponding constant for a multi-recombinative $(\mu/\mu_I, \lambda)$-ES. Furthermore, the self-adaptation on the (unbounded) ridge function has been investigated in [12] deriving a steady-state progress rate. The ellipsoid model in [13] yields τ proportional to the square root of the ratio of the smallest eigenvalue to the sum of the eigenvalues of the Hessian, thus resulting in $\tau(N)$ decreasing faster than $1/\sqrt{N}$.

In this paper, the first analysis of self-adaptation on a highly multimodal function, i.e., the Rastrigin function, is conducted. Multimodality poses a major challenge for the σ-adaptation. Slow adaptation usually improves the success rate of global convergence due to higher robustness [3]. This, however, is detrimental to the search efficiency. In this work, a theoretical approach is introduced to model and predict the mutation strength change under high multimodality. It will enable to tune the self-adaptation on Rastrigin to maximize its efficiency.

In Sec. II the Rastrigin function and the multi-recombinative $(\mu/\mu_I, \lambda)$-σSA-ES are introduced. In Sec. III one-generation performance measures are defined and preliminary results are stated, which are necessary for a complete modeling of the ES. In Sec. IV the dynamic model of the ES is introduced. The self-adaptation response function is derived in Sec. V-A in the limit of infinitely large populations. Then, in Sec. V-B, the learning parameter τ for the self-adaptation on the Rastrigin function is derived. In Sec. VI the efficiency of the σSA-ES is experimentally evaluated and compared to the theoretical prediction. Finally, conclusions are drawn in Sec. VII. Note that a list of all introduced variables is included in the

Manuscript received MMMMMMM, YYYY; revised MMMMMMM, YYYY; accepted MMMMMMM, YYYY. Date of publication MMMMMMM, YYYY; date of current version MMMMMMM, YYYY. This research was funded by the Austrian Science Fund (FWF) under grant P33702-N. For open access purposes, the author has applied a CC BY public copyright license to any author accepted manuscript version arising from this submission. The authors gratefully thank Lisa Schönenberger for providing valuable feedback.

The authors are with the Research Center Business Informatics, Vorarlberg University of Applied Sciences, 6850 Dornbirn, Austria (e-mail: amir.omeradzic@fhv.at, hans-georg.beyer@fhv.at).

This article has supplementary downloadable material and color versions of the figures available online at https://doi.org/XX.XXXX/TEVC.XXXX.XXXXXXX.

Digital Object Identifier XX.XXXX/TEVC.XXXX.XXXXXXX

This work is licensed under a Creative Commons Attribution 4.0 License. For more information, see https://creativecommons.org/licenses/by/4.0/

Algorithm 1 $(\mu/\mu_I, \lambda)$-σSA-ES

1: $g \leftarrow 0$
2: initialize $\left(\mathbf{y}^{(0)}, \sigma^{(0)}\right)$
3: **repeat**
4: **for** $l = 1, ..., \lambda$ **do**
5: $\tilde{\sigma}_l \leftarrow \sigma^{(g)} \mathrm{e}^{\tau \mathcal{N}_l(\mathbf{0},\mathbf{1})}$
6: $\tilde{\mathbf{x}}_l \leftarrow \tilde{\sigma}_l \mathcal{N}_l(\mathbf{0}, \mathbf{1})$
7: $\tilde{\mathbf{y}}_l \leftarrow \mathbf{y}^{(g)} + \tilde{\mathbf{x}}_l$
8: $\tilde{f}_l \leftarrow f(\tilde{\mathbf{y}}_l)$
9: **end for**
10: $(\tilde{f}_{1;\lambda}, ..., \tilde{f}_{m;\lambda}, ..., \tilde{f}_{\mu;\lambda}) \leftarrow \mathrm{sort}(\tilde{f}_1, ..., \tilde{f}_\lambda)$
11: $\mathbf{y}^{(g+1)} \leftarrow \frac{1}{\mu} \sum_{m=1}^{\mu} \tilde{\mathbf{y}}_{m;\lambda}$
12: $\sigma^{(g+1)} \leftarrow \frac{1}{\mu} \sum_{m=1}^{\mu} \tilde{\sigma}_{m;\lambda}$
13: $g \leftarrow g + 1$
14: **until** termination criterion

supplementary material in Table I.

II. Test Function and Evolution Strategy

The Rastrigin test function f is defined in N dimensions for a real-valued search vector $\mathbf{y} = [y_1, ..., y_N]$ as

$$f(\mathbf{y}) \coloneqq \sum_{i=1}^{N} \left[y_i^2 + A(1 - \cos(\alpha y_i)) \right], \tag{1}$$

with oscillation amplitude A and frequency α (default value $\alpha = 2\pi$ is used throughout the paper). Minimization of f is considered with the global minimizer located at $\hat{\mathbf{y}} = \mathbf{0}$. Given A and α, the function has a finite number of local attractors in each dimension, such that the overall number of local minima scales exponentially with N. The Rastrigin function has a quadratic global structure and the convergence of the ES on f is evaluated using the residual distance R defined as $R^2 \coloneqq \sum_i y_i^2$.

The Rastrigin function is investigated using a $(\mu/\mu_I, \lambda)$-ES, see Algorithm 1, with μ parents, λ offspring, intermediate multi-recombination, and generation counter g. The selection pressure (or truncation ratio) is defined as $\vartheta \coloneqq \mu/\lambda$. Isotropic normally distributed mutations of strength σ are applied and σ is adapted using self-adaptation by sampling log-normally distributed values for each offspring (Lines 5-7), see also density (29). The adaptation is tuned via the learning parameter τ. Smaller τ-values yield a slower, more robust adaptation. Larger values result in faster, more efficient, but less robust adaptation. The default value for τ was derived in [12] on the sphere in the limit $N \to \infty$ as $\tau = 1/\sqrt{2N}$. On the Rastrigin function one observes a higher success probability P_S of Alg. 1 if smaller values for τ are chosen. The τ-dependence will be investigated further throughout the paper.

III. Definitions and Preliminary Results

In this section the local performance measures will be defined, which will be necessary for the dynamic model presented in Sec. IV. As the focus of this paper is the investigation of the self-adaptation, important preliminary results will also be stated here.

A. Local Performance Measures

The strategy's local performance in search space can be measured using the so-called progress rate (denoted by φ). The first-order i-th component progress rate φ_i is defined as the expected value (given position $\mathbf{y}$ and mutation strength σ)

$$\varphi_i \coloneqq \mathrm{E}\left[y_i^{(g)} - y_i^{(g+1)} \,\middle|\, \mathbf{y}^{(g)}, \sigma^{(g)} \right]. \tag{2}$$

Analogous to (2) a second-order progress along the i-th component is defined by squaring the values as

$$\varphi_i^{\mathrm{II}} \coloneqq \mathrm{E}\left[(y_i^{(g)})^2 - (y_i^{(g+1)})^2 \,\middle|\, \mathbf{y}^{(g)}, \sigma^{(g)} \right]. \tag{3}$$

φ_i^{II} was first introduced in [13] analyzing self-adaptation on the ellipsoid model. The first order φ_i can be used if comparably small mutation strengths σ are used relative to the residual distance R. For larger mutation strengths the ES performs large steps, such that y_i often changes its sign between generations. In this case, φ_i^{II} is necessary for a more accurate model of progress towards the optimizer as it can be approached independent of the sign of y_i. φ_i^{II} measures the progress of single components, while global convergence is measured (usually) as a function of the residual distance R. One can think of examples where global progress ($R^{(g+1)} < R^{(g)}$) occurs with some components having $\varphi_i^{\mathrm{II}} > 0$ and others showing $\varphi_i^{\mathrm{II}} < 0$, such that demanding $\varphi_i^{\mathrm{II}} > 0$ for all i would be too restrictive. Therefore, an additional aggregation step is needed to obtain an R-dependent measure. Summing over (3) and using $R^2 = \sum_i y_i^2$, one defines [4]

$$\sum_{i=1}^{N} \varphi_i^{\mathrm{II}} = \mathrm{E}\left[(R^{(g)})^2 - (R^{(g+1)})^2 \middle| R^{(g)}, \sigma^{(g)} \right] =: \varphi_R^{\mathrm{II}}. \tag{4}$$

The evaluation of (4) is done in Sec. III-B. It is important to note that all progress rates above will be evaluated asymptotically in the limit $\tau \to 0$. This has two reasons. First, the evaluation of the expected values proves to be very hard, if not impossible, when $\tau > 0$ is chosen. Second, to obtain closed-form solutions of the self-adaptation response (SAR) at all, the limit $\tau \to 0$ is also needed.

The SAR, denoted by the symbol ψ, measures the relative change of the mutation strength σ and is defined as

$$\psi \coloneqq \mathrm{E}\left[(\sigma^{(g+1)} - \sigma^{(g)})/\sigma^{(g)} \,\middle|\, \mathbf{y}^{(g)}, \sigma^{(g)} \right]. \tag{5}$$

The evaluation of all progress rates and the SAR requires to model the selection process of the ES. To this end, one defines the quality gain Q at location $\mathbf{y}$ due to isotropic mutation $\mathbf{x} \sim \sigma\mathcal{N}(\mathbf{0}, \mathbf{1})$ as the local fitness change

$$Q \coloneqq f(\mathbf{y} + \mathbf{x}) - f(\mathbf{y}). \tag{6}$$

As the quality gain is a random variate, a probabilistic model for the distribution of Q is required. The cumulative distribution function (CDF) of Q is denoted as P_Q. Exact solutions for P_Q cannot be obtained due to the underlying structure of (1) as it contains sums over trigonometric and squared random variates. However, based on the idea of the central limit theorem (CLT), one can apply a normal approximation of the quality gain distribution for comparably large N (see discussion in [15]). While the applicability of

the CLT cannot be rigorously proven, experiments do show very good agreement. The normality assumption is therefore not critical for the further analysis. Using expected value $E_Q := \mathrm{E}[Q]$ and variance $D_Q^2 := \mathrm{Var}[Q]$, one approximates P_Q using the standard normal CDF $\Phi(\cdot)$ as

$$\widetilde{P}_Q = \Phi\left(\frac{q - E_Q}{D_Q}\right). \tag{7}$$

Expected value and variance in (7) are evaluated in [15] as functions of the Rastrigin parameters and mutation strength σ. One has [15, (30)]

$$E_Q(\mathbf{y}) = \sum_{i=1}^{N}\left[\sigma^2 + A\cos(\alpha y_i)\left(1 - \mathrm{e}^{-\frac{(\alpha\sigma)^2}{2}}\right)\right], \tag{8}$$

and the variance is evaluated as [15, (31)]

$$\begin{aligned} D_Q^2(\mathbf{y}) = \sum_{i=1}^{N}\Big\{ & 4\sigma^2 y_i^2 + 2\sigma^4 \\ & + \frac{A^2}{2}\left(1 - \mathrm{e}^{-(\alpha\sigma)^2}\right)\left(1 - \cos(2\alpha y_i)\mathrm{e}^{-(\alpha\sigma)^2}\right) \\ & + 2A\alpha\sigma^2\mathrm{e}^{-\frac{1}{2}(\alpha\sigma)^2}\left(\alpha\sigma^2\cos(\alpha y_i) + 2y_i\sin(\alpha y_i)\right)\Big\}. \end{aligned} \tag{9}$$

Based on the quality gain distribution (7), progress rates φ_i and φ_i^{II} have been derived in [15]. For the further analysis only second order φ_i^{II} is needed. It was derived in [15, p. 24] assuming $\mu, \lambda, N \to \infty$ (constant ϑ) as

$$\varphi_i^{\mathrm{II}} \simeq c_\vartheta \frac{\sigma^2}{D_Q}\left(4y_i^2 + \mathrm{e}^{-\frac{1}{2}(\alpha\sigma)^2}2\alpha A y_i \sin(\alpha y_i)\right) - \frac{\sigma^2}{\mu}. \tag{10}$$

Note that the exponential function in (10) models the limited range of local attraction. Additionally, the asymptotic generalized progress coefficients $e_\vartheta^{a,b}$ were derived [15, (45)] for $a \geq 1$, $b \geq 0$ as

$$e_\vartheta^{a,b} := \left(\mathrm{e}^{-\frac{1}{2}\left[\Phi^{-1}(\vartheta)\right]^2}/(\sqrt{2\pi}\vartheta)\right)^a\left(-\Phi^{-1}(\vartheta)\right)^b, \tag{11}$$

with the special case $c_\vartheta := e_\vartheta^{1,0}$ used in (10). They correspond to the generalized progress coefficients $e_{\mu,\lambda}^{a,b}$ of [7, (5.112)] in the limit of infinitely large population size. Φ^{-1} denotes the quantile function of the standard normal distribution.

B. Component Aggregation

As already discussed above (4), the aggregation of all component-wise φ_i^{II} is needed for a global (R^2-dependent) progress rate. This method will be useful to model the dynamics of the ES as a function of the residual distance R, see (23). Furthermore, some important relations to the sphere function can be established easily.

Starting from (4), the evaluation of $\sum_i \varphi_i^{\mathrm{II}}(\mathbf{y})$ given some value for $R^2 = \sum_i y_i^2$ is not trivial as terms containing trigonometric functions in y_i appear. Since analytic averaging is intractable for $N \geq 3$, a stochastic averaging method was introduced. This issue was discussed in [4]. Stochastic averaging assumes that the components y_i are random i.i.d. variates distributed normally around the global optimizer $\hat{\mathbf{y}} = 0$ for any g, such that

$$y_i \sim \mathcal{N}(0, R^2/N). \tag{12}$$

Note that the expectation of the sum over squared components yields $\mathrm{E}\left[\sum_i y_i^2\right] = R^2$. By assumption (12) each component contributes roughly as $y_i^2 \approx R^2/N$ to the residual distance R^2. Using random variates (12) the sums over trigonometric functions can be approximated by their corresponding expected values (applying the CLT for $N \to \infty$), such that the aggregated progress rate is derived as [4, (35)]

$$\varphi_R^{\mathrm{II}} = c_\vartheta \frac{2R^2\sigma^2}{D_Q(R)}\left(2 + \alpha^2 A\mathrm{e}^{-\frac{\alpha^2}{2}\left(\sigma^2 + \frac{R^2}{N}\right)}\right) - N\frac{\sigma^2}{\mu}. \tag{13}$$

Result (13) is now R^2-dependent and contains the (aggregated) information of N progress rates. Using the same approach, the aggregated (averaged) quality gain variance $D_Q^2(R)$ is derived from $D_Q(\mathbf{y})$ in (9), such that one obtains [4, (36)]

$$\begin{aligned} D_Q^2(R) = {} & 4R^2\sigma^2 + 2N\sigma^4 + \\ & + \frac{NA^2}{2}\left(1 - \mathrm{e}^{-(\alpha\sigma)^2}\right)\left(1 - \mathrm{e}^{-\alpha^2\left(\sigma^2 + 2\frac{R^2}{N}\right)}\right) \\ & + 2NA\alpha^2\sigma^2\mathrm{e}^{-\frac{\alpha^2}{2}\left(\sigma^2 + \frac{R^2}{N}\right)}\left(\sigma^2 + 2\frac{R^2}{N}\right). \end{aligned} \tag{14}$$

Similarly, the aggregated (averaged) expectation value $E_Q(R)$ is derived from $E_Q(\mathbf{y})$ in the supplementary material B-A

$$E_Q(R) = N\sigma^2 + NA\mathrm{e}^{-\frac{1}{2}\frac{(\alpha R)^2}{N}}\left(1 - \mathrm{e}^{-\frac{(\alpha\sigma)^2}{2}}\right). \tag{15}$$

The results (13) and (14) can be readily used to obtain the sphere quality gain $\mathrm{E}\left[(R^{(g)})^2 - (R^{(g+1)})^2\right]$ as a special case by setting $A = 0$ (or $\alpha = 0$). The sphere is considered here as it provides similarities in the dynamical behavior compared to the Rastrigin function. The sphere progress rate is defined as $\varphi := \mathrm{E}\left[R^{(g)} - R^{(g+1)}\right]$. By introducing normalizations (denoted by $*$) as $\varphi^* = \varphi N/R$ and $\varphi_R^{\mathrm{II},*} = \varphi_R^{\mathrm{II}} N/(2R^2)$, see [16, p. 16], the asymptotic equality ($N \to \infty$) holds

$$\varphi^* \simeq \varphi_R^{\mathrm{II},*}, \tag{16}$$

which yields the sphere progress rate (setting $A = 0$)

$$\varphi_{\mathrm{sph}}^* = \frac{c_\vartheta \sigma^*}{\sqrt{1 + \sigma^{*2}/2N}} - \frac{\sigma^{*2}}{2\mu}. \tag{17}$$

Equation (17) is a function of the scale-invariant mutation strength σ^*, which is obtained by normalizing σ with dimension N and residual distance R according to

$$\sigma^* = \sigma N/R. \tag{18}$$

On the sphere one has $\varphi_{\mathrm{sph}}^* > 0$ for any $\sigma^* \in (0, \sigma_{\varphi_0}^*)$, where $\sigma_{\varphi_0}^*$ denotes the (second) zero of φ_{sph}^*. It was evaluated in [4, (41)] as

$$\sigma_{\varphi_0}^* = \left[\left(N^2 + 8Nc_\vartheta^2\mu^2\right)^{1/2} - N\right]^{1/2}. \tag{19}$$

Depending on the choice of learning parameter τ, a constant steady-state σ^*-level (in expectation) is attained on the sphere. This results in a constant scale-invariant progress rate (17) for given N, μ, and ϑ, see e.g. Fig. 2. On the Rastrigin function the condition $\sigma^* \in (0, \sigma_{\varphi_0}^*)$ also holds due to its quadratic global structure. Furthermore, small τ raise the steady-state σ^*-level closer to $\sigma_{\varphi_0}^*$, which increases the success rate at the expense of having a lower efficiency. This will be important for the derivation of an efficient τ in Sec. V-B.

IV. Dynamics and Steady-State

The progress rate and SAR (defined in Sec. III) model the expected change of $\mathbf{y}$ and σ between two generations. We are interested in modeling and predicting the dynamics of the σSA-ES over many generations to investigate its convergence properties. An established method is the dynamical systems approach introduced in [7, Ch. 7]. It enables to test the analytically obtained formulas against actual optimization runs over many generations. Furthermore, steady-state conditions of the dynamic system can be derived. This section outlines the overall goal. The derivation of required quantities follows in the subsequent sections.

Starting with the second order progress rate (3), one can rearrange the equation in terms of an iterative mapping $g \to g+1$ for the i-th component as

$$(y_i^{(g+1)})^2 = (y_i^{(g)})^2 - \varphi_i^{\mathrm{II}}(\sigma^{(g)}, \mathbf{y}^{(g)}) + \epsilon_y(\sigma^{(g)}, \mathbf{y}^{(g)}), \quad (20)$$

with the random variate ϵ_y modeling fluctuations in the search space. Analogously, the definition (5) of the SAR-function is rearranged giving an iterative mapping

$$\sigma^{(g+1)} = \sigma^{(g)}(1 + \psi(\sigma^{(g)}, \mathbf{y}^{(g)})) + \epsilon_\sigma(\sigma^{(g)}, \mathbf{y}^{(g)}), \quad (21)$$

with ϵ_σ modeling the fluctuations of the σ-adaptation. As φ_i^{II} and ψ are expected values of their respective quantities, it holds $\mathrm{E}[\epsilon_y] = \mathrm{E}[\epsilon_\sigma] = 0$. For the subsequent investigations the fluctuation terms will be neglected by setting $\epsilon_y = \epsilon_\sigma = 0$. This assumption is a simplification, resulting in a deterministic iteration. However, it will be compared with averaged dynamics of real optimization runs, showing a good agreement. One obtains the evolution equations of the $\mathbf{y}$-dependent iteration as

$$\begin{aligned}(y_i^{(g+1)})^2 &= (y_i^{(g)})^2 - \varphi_i^{\mathrm{II}}(\sigma^{(g)}, \mathbf{y}^{(g)}) \\ \sigma^{(g+1)} &= \sigma^{(g)}(1 + \psi(\sigma^{(g)}, \mathbf{y}^{(g)})),\end{aligned} \quad (22)$$

with $i = 1, ..., N$, which yields a set of $N+1$ equations to be iterated. It will be abbreviated as "$\mathbf{y}$-iteration". Note that both $\varphi_i^{\mathrm{II}}(\mathbf{y})$ and $\psi(\mathbf{y})$ are even functions of y_i, such that taking the square-root of $(y_i^{(g+1)})^2$ does not pose an issue.

Using the same argumentation as for (20), one can define R^2-dependent evolution equations using (4) and $\psi(\sigma, R)$

$$\begin{aligned}(R^{(g+1)})^2 &= (R^{(g)})^2 - \varphi_R^{\mathrm{II}}(\sigma^{(g)}, R^{(g)}) \\ \sigma^{(g+1)} &= \sigma^{(g)}(1 + \psi(\sigma^{(g)}, R^{(g)})),\end{aligned} \quad (23)$$

which reduces the number of equations from $N+1$ in (22) to two. It will be abbreviated as "R-iteration" and further investigated in Sec. V-B.

A goal of the analysis is to derive a steady-state condition for the evolution of scale-invariant σ^*. Note that σ^* rescales σ by the current residual distance R (and N), see (18). For $\mathbf{y}$-iteration (22) there are N positional coordinates to be evaluated. The steady-state analysis of the $N+1$ dimensional system is not tractable, such that the focus is set on R-iteration (23). Recalling that $\varphi = \mathrm{E}\left[R^{(g)} - R^{(g+1)}\right]$, $\varphi^* = \varphi N/R$, and $\varphi^* \simeq \varphi_R^{\mathrm{II},*}$, R-iteration (23) is re-formulated using (18) as

$$R^{(g+1)} = R^{(g)}\left(1 - \varphi_R^{\mathrm{II},*}/N\right) \quad (24)$$

$$\sigma^{*,(g+1)} R^{(g+1)}/N = (\sigma^{*,(g)} R^{(g)}/N)(1+\psi). \quad (25)$$

Inserting (24) into (25) yields the σ^*-evolution equation

$$\sigma^{*,(g+1)} = \sigma^{*,(g)}(1+\psi)/(1 - \varphi_R^{\mathrm{II},*}/N). \quad (26)$$

Imposing the steady-state condition $\sigma_{ss}^* = \sigma^{*,(g+1)} = \sigma^{*,(g)}$ and noting that in the general case $\varphi_R^{\mathrm{II},*} = \varphi_R^{\mathrm{II},*}(\sigma_{\mathrm{ss}}^*, R)$ and $\psi = \psi(\sigma_{\mathrm{ss}}^*, R, \tau)$, one has

$$\varphi_R^{\mathrm{II},*}(\sigma_{\mathrm{ss}}^*, R) = -N\psi(\sigma_{\mathrm{ss}}^*, R, \tau). \quad (27)$$

On the sphere function one has scale-invariant progress $\varphi_R^{\mathrm{II},*}(\sigma^*)$ and self-adaptation $\psi(\sigma^*, \tau)$, such that (27) yields the simplified condition (analogous to [7, (7.162)])

$$\varphi_R^{\mathrm{II},*}(\sigma_{\mathrm{ss}}^*) = -N\psi(\sigma_{\mathrm{ss}}^*, \tau). \quad (28)$$

If a closed-form solution of (27) were available, one could predict the steady-state $\sigma_{\mathrm{ss}}^*(R, \tau)$ at any residual distance R given some τ. Additionally, one could analyze the functional dependency between τ, fitness-, and strategy-parameters in the steady-state. However, as discussed later in Sec. V-B, there is no closed-form solution of (27) for Rastrigin. Furthermore, a resulting τ should be scale-invariant (independent of R) according to (28) to guarantee good performance on the sphere, which is the global structure of Rastrigin. Conditions for a steady-state σ_{ss}^* are discussed in Sec. V-B showing that scale-invariance cannot be achieved on Rastrigin. Instead, a "critical" σ_{crit}^* is derived, which characterizes the Rastrigin-specific dynamics well in terms of the sphere steady-state. It will enable to solve (28) for learning parameter τ, which in turn enables us to tune the self-adaptation of the ES.

V. Self-Adaptation

The progress rates defined in Sec. III determine the expected positional change given $\sigma^{(g)}$. A full description of the self-adaptive σSA-ES requires the evaluation of the σ-change using the SAR function defined in (5), which is done now.

A. Self-Adaptation Response (SAR)

For the $(\mu/\mu_I, \lambda)$-σSA-ES, $\sigma^{(g)}$ denotes the recombined mutation strength of the $m = 1, ..., \mu$ selected values (see Alg. 1, Line 12). From now on the conditional variables $\mathbf{y}^{(g)}$ and $\sigma^{(g)}$ are implicitly assumed to be given and $\sigma = \sigma^{(g)}$ is used for brevity. Random mutations $\tilde{\sigma}$ are sampled according to the probability density of the log-normal mutation operator $p_\sigma(s)$, see Line 5. It is defined in terms of learning parameter τ given mutation strength σ for $s \in (0, \infty)$ as

$$p_\sigma(s) \coloneqq \frac{1}{\sqrt{2\pi}\tau s} \exp\left[-\frac{1}{2}\left(\frac{\ln(s/\sigma)}{\tau}\right)^2\right]. \quad (29)$$

First, expected value (5) after selection and recombination can be rewritten in terms of an order statistic density $p_{m;\lambda}$ for the m-th best individual as

$$\psi = \frac{1}{\mu}\sum_{m=1}^{\mu}\int_0^\infty \left(\frac{s-\sigma}{\sigma}\right) p_{m;\lambda}(s|\sigma)\,\mathrm{d}s\,. \quad (30)$$

Equation (30) was evaluated on the sphere in [12] in the asymptotic limits $N \to \infty$ ($\mu \ll N$) and $\tau \to 0$. In this paper a slightly different approach is taken. As the progress

rate (10) was derived for large populations $\mu,\lambda \to \infty$ (constant $\vartheta = \mu/\lambda$), the goal is to obtain a corresponding SAR for infinitely large populations. The details of the derivation are presented in Appendix A. To this end, a large population identity is applied and the limit $\tau \to 0$ is assumed to provide a closed-form solution. The final result (A.20) yields

$$\psi \simeq \tau^2 \left(\frac{1}{2} - c_\vartheta \sigma \frac{E'_Q(\sigma)}{D_Q(\sigma)} + e_\vartheta^{1,1} \sigma \frac{D'_Q(\sigma)}{D_Q(\sigma)} \right). \tag{31}$$

Result (31) has interesting properties. It is a generic expression for which the positional dependency and the test function parameters are contained within E_Q, D_Q, and its corresponding derivatives. The population dependence is included solely in the coefficients c_ϑ and $e_\vartheta^{1,1}$. Furthermore, it can be mapped directly to result [12, (C.23)], where the derivation of ψ was performed for finite μ and λ giving $\psi \simeq \tau^2(\frac{1}{2} - c_{\mu/\mu,\lambda}\sigma E'_Q/D_Q + e_{\mu,\lambda}^{1,1}\sigma D'_Q/D_Q)$. Note that the same functional dependencies are obtained with the large population limit only affecting the coefficients giving $e_{\mu,\lambda}^{a,b} \to e_\vartheta^{a,b}$. This transformation of progress coefficients into their asymptotic form was also observed for the progress rates in [15].

The evaluation of ψ on the Rastrigin function requires to insert E_Q and D_Q^2 (with respective derivatives) into (31). As the results are very lengthy, this step is omitted for better readability. However, the expressions will be evaluated during subsequent experiments. The SAR as a function of $\mathbf{y}$ and R, respectively, yields

$$\psi(\mathbf{y}) \simeq \tau^2 \left(\frac{1}{2} - c_\vartheta \sigma \frac{E'_Q(\mathbf{y})}{D_Q(\mathbf{y})} + e_\vartheta^{1,1} \sigma \frac{D'_Q(\mathbf{y})}{D_Q(\mathbf{y})} \right) \tag{32}$$

$$\psi(R) \simeq \tau^2 \left(\frac{1}{2} - c_\vartheta \sigma \frac{E'_Q(R)}{D_Q(R)} + e_\vartheta^{1,1} \sigma \frac{D'_Q(R)}{D_Q(R)} \right), \tag{33}$$

with $E_Q(\mathbf{y})$ (8), $D_Q^2(\mathbf{y})$ (9), $E_Q(R)$ (15), and $D_Q^2(R)$ (14). For (32) and (33) the σ-dependence is implicitly assumed to be given and the derivative is taken w.r.t. σ. At this point one-generation experiments are conducted to evaluate the theoretical prediction for ψ. To this end, single optimization steps are performed and (5) is averaged over 10^5 trials. The results are then compared to closed-form results (32) and (33).

Figure 1a shows ψ for two different random realizations of $\mathbf{y}$ chosen to illustrate the effects of local attraction. Very good agreement between simulation and $\psi(\mathbf{y})$ can be observed, while $\psi(R)$ shows larger deviations for smaller σ. Given very small σ, ψ is always positive. In this case, the explored search space region is very small and test functions can be approximated by a hyperplane. For moderate $\sigma < 0.5$ a larger region of the function is explored and local attraction (or repulsion in the case of a local maximum) effects are prominent. On the left side $\psi(\mathbf{y})$ increases from its initial value, indicating that selected individuals have larger sampled $\tilde{\sigma}$. This occurs, for example, when the ES is close to a local maximum. On the right side $\psi(\mathbf{y})$ drops significantly for moderate σ, which indicates local attraction effects and smaller sampled $\tilde{\sigma}$. $\psi(R)$ does not model local attraction correctly as it evaluates an average response at $\|\mathbf{y}\| = R$ and no specific location $\mathbf{y}$ (fixed in the experiment). In real optimization runs (at small σ), one observes that component aggregation (12)

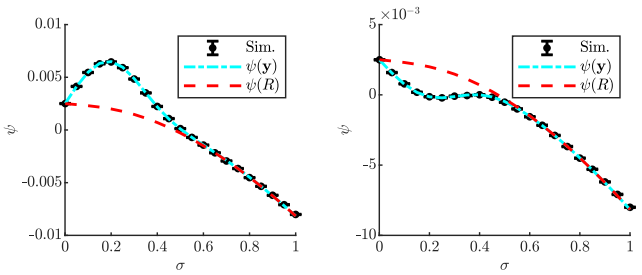

(a) $\psi(\sigma)$ with left and right plots showing different random $\mathbf{y}$-realizations given the same R.

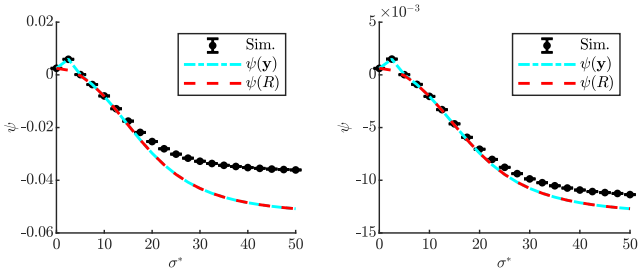

(b) $\psi(\sigma^*)$ as a function of $\sigma^* = \sigma N/R$, see (18), for $\tau = 1/\sqrt{2N}$ (left) and $\tau = 1/\sqrt{8N}$ (right).

Fig. 1: One-generation experiments for ψ with $(100/100_I, 200)$-ES, $A = 10$, $N = 100$, initialized at random $\mathbf{y}$ with $\|\mathbf{y}\| = R = \sqrt{N}$, where local attraction is present. Simulations of (5) are displayed as black dots (vanishing error bars, 10^5 trials). Closed-form result (32) is shown in dash-dotted cyan and (33) in dashed red.

is violated and the y_i are not isotropically distributed due to local attraction. For large $\sigma > 0.5$, however, $\psi(\mathbf{y})$ and $\psi(R)$ are very similar. The reason is that the global structure of the Rastrigin function, i.e., the sphere, becomes dominating. In this case, (12) holds, which corresponds to a global search of the ES. This observation suggests displaying $\psi(\sigma^*)$ as a function of the scale-invariant mutation strength (18).

Figure 1b shows $\psi(\sigma^*)$ for two values of τ. The range of σ^* was chosen large enough to cover the range of positive progress on the sphere, which is defined by $\sigma^* < \sigma^*_{\varphi_0}$ in (19). One observes larger deviations of the derived result if τ is chosen larger (left plot), which was expected. Most of the deviations are due to Taylor expansion (A.15) and neglecting higher orders of $O\left(\tau^4\right)$. Since $\psi(R)$ represents an aggregated measure over all y_i-components with $\|\mathbf{y}\| = R$, it can be regarded as an average value. For moderate and large σ^* the deviations between $\psi(\mathbf{y})$ and $\psi(R)$ vanish and local attraction is negligible (analogous to Fig. 1a). One may conclude that $\psi(R)$ yields good agreement with experiments for sufficiently large σ^*, where the spherical structure of Rastrigin is dominating.

The conducted experiments show that $\psi(\mathbf{y})$ yields very good agreement provided that τ is relatively small. It also models the SAR in the presence of local attraction. This also holds well for moderately large N and μ. On the other hand, $\psi(R)$ significantly simplifies the positional dependence (from N components to one). Experiments show its limitations when predicting local attraction effects for very small σ^*, but it

This article has been accepted for publication in IEEE Transactions on Evolutionary Computation. This is the author's version which has not been fully edited and content may change prior to final publication. Citation information: DOI 10.1109/TEVC.2024.3400857

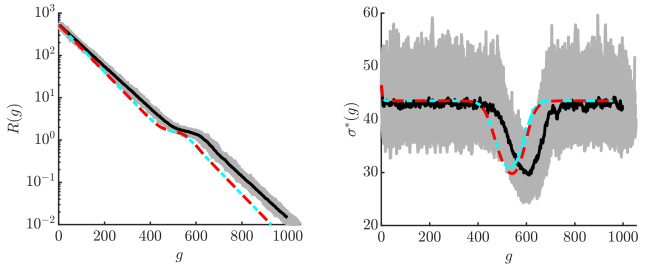

(a) Parameter $A = 1$ giving $P_S = 1$.

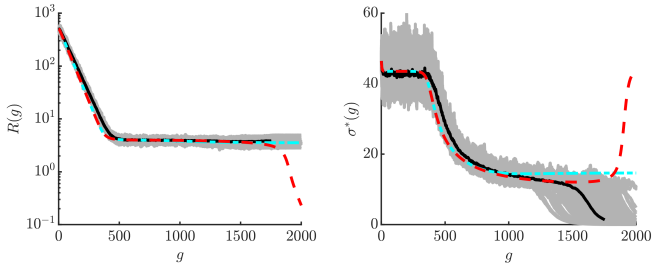

(b) Parameter $A = 7$ giving $P_S = 0$.

Fig. 2: Dynamics of R and σ^* (100 trials of Alg. 1) for $(100/100_I, 200)$-ES, $N = 100$, $\tau = 1/\sqrt{8N}$ and varying A (median: solid black; individual trials: solid gray). The cyan dash-dotted line shows (22), and the red dashed line (23). The runs are initialized outside the local attraction region.

yields good results for larger σ^*-values.

B. Dynamics and τ-Derivation

The one-generation experiments of the last section have shown good agreement with simulations. Now the results for $\psi(\mathbf{y})$ and $\psi(R)$ are tested over many generations using iterations (22) and (23). The experiments in Fig. 2 show the $R(g)$- and $\sigma^*(g)$-dynamics of real optimization runs (Alg. 1) compared to iterated dynamics. The median is taken as a measure of central tendency as it is more stable w.r.t. outliers compared to the mean. Depending on the chosen Rastrigin parameter A, one observes globally (Fig. 2a) and locally converging (Fig. 2b) runs with measured success rate P_S. A characteristic drop (and rise) of $\sigma^*(g)$ is observed. Both iterations show good agreement w.r.t. the measured median dynamics. Despite R-iteration being aggregated over all N components, it shows similar results to $\mathbf{y}$-iteration. Larger deviations occur in Fig. 2b during the phase of local convergence at $g \geq 1000$, where $\sigma^* \to 0$. This would be critical if P_S were evaluated for the iterations. In our case, the focus is set on the investigation of the observed σ^*-decrease.

Figure 3 shows the progress landscape $\varphi_R^{\mathrm{II},*}(\sigma^*, R)$, see (13) with $\varphi_R^{\mathrm{II},*} = \varphi_R^{\mathrm{II}} N/(2R^2)$, for the same configurations as shown in Fig. 2. The dynamics are overlaid and g is implicitly given. The σ^*-bound was chosen slightly larger than $\sigma^*_{\varphi_0}$ (range of positive progress), see (19), and $R \in [10^{-1}, 10^2]$ to provide good visibility of the relevant characteristics. White regions correspond to high $\varphi_R^{\mathrm{II},*}$ and dark regions to low $\varphi_R^{\mathrm{II},*}$ (zero-progress-line shown in bold white). Thin black lines are levels of equal progress. For $R \to \infty$ and $R \to 0$ the

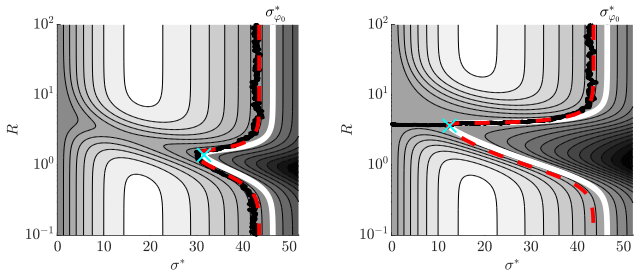

Fig. 3: Progress rate $\varphi_R^{\mathrm{II},*}(\sigma^*, R)$ is shown, see (13), for the configuration of Fig. 2 with $A = 1$ (left) and $A = 7$ (right). The median of real ES-dynamics is displayed in solid black. The iterated dynamics of (23) is shown in dashed red. σ^*_{crit} from (34) is marked in cyan as "×". $\sigma^*_{\varphi_0}$ from (19) is marked at the top right. $\varphi_R^{\mathrm{II},*}(\sigma^*, R)$ and $\psi(\sigma^*, R)$ are displayed in color for $A = 1$ in the supplementary material B-B.

sphere function is recovered (see vertical lines indicating scale-invariance). On the left, the ES moves around a characteristic "progress dip" (see also [4]), which leads to the σ^*-reduction. The reduction is required to maintain positive progress. On the right, local convergence occurs as $\sigma^* \to 0$ ($R > 0$). The observed dip is an effect of the presence of many local attractors acting similar to noise during the selection. It slows down the strategy's progress significantly. The ES reduces its mutation strength from its sphere steady-state value σ^*_{ss} reaching the vicinity of a critical value σ^*_{crit}. It is defined as

$$\sigma^*_{\mathrm{crit}} := \min_R \sigma^*, \quad \text{such that} \quad \varphi_R^{\mathrm{II},*} = 0. \tag{34}$$

σ^*_{crit} is displayed in Fig. 3 and changes with the fitness parameters. There are two possible outcomes when σ^* reaches σ^*_{crit}. In Fig. 3 (left), one observes global convergence and σ^* increases again to the steady-state σ^*_{ss}. In Fig. 3 (right), local convergence occurs due to significantly higher multimodality (larger A), such that $\sigma^* \to 0$.

A slower adaptation with $\tau = 1/\sqrt{8N}$ (instead of $\tau = 1/\sqrt{2N}$), see also Fig. 5, helps to maintain high σ^*-levels. It also improves the success rate P_S compared to larger choices of τ by keeping the mutation strength large. The major downside is that any σ^*-change is slow. This holds especially when σ^* is decreased to reach σ^*_{crit} and then increased again. In the following, the approach will be to improve the adaptation efficiency. The goal is to decrease the σ^*_{ss}-level by choosing a larger τ, such that σ^*_{ss} lies in the vicinity of σ^*_{crit}. To this end, an approximation for σ^*_{crit} will be derived first. Then, one may set $\sigma^*_{\mathrm{ss}} = \sigma^*_{\mathrm{crit}}$ in (28), demanding a steady-state on the sphere, i.e., on the global structure of Rastrigin. Finally, (28) can be solved and an expression for $\tau = \tau(N, \alpha, A)$ is obtained. Choosing $\tau(N, \alpha, A)$ the ES approaches (approximately) the region of the progress dip with $\sigma^*_{\mathrm{ss}} \approx \sigma^*_{\mathrm{crit}}$. This will improve the search efficiency but decrease the success rate P_S due to smaller mutation strengths. However, provided that the population size is chosen large enough, one can maintain $P_S > 0$.

First, condition (28) is evaluated for the sphere by inserting progress rate (17) and SAR (33). The derivation is straight-

forward and can be found in the supplementary material B-C. It relies on setting $A = 0$ in (14) and (15), and evaluating expected derivatives. The obtained expressions are further simplified by assuming large populations with $\sqrt{N} \ll \mu$, such that the steady-state condition on the sphere yields

$$c_\vartheta \sqrt{2N} - \frac{\sigma_{\mathrm{ss}}^{*2}}{2\mu} = -N\tau^2 \left(\frac{1}{2} - c_\vartheta \sqrt{2N} + 2e_\vartheta^{1,1} \right). \tag{35}$$

A closed-form solution for σ^*_{crit} can only be obtained under certain simplifications. The residual distance R at which σ^* decreases (see Fig. 4, right) can be approximated using the Rastrigin maximum noise strength $\sigma_\epsilon^2 \coloneqq NA^2/2$ as [3]

$$R_\infty^2 = \sigma_\epsilon N/(4c_\vartheta \mu) = N^{3/2} A/(\sqrt{32} c_\vartheta \mu). \tag{36}$$

R_∞ is obtained in [4] using a simplified variance (14) by setting all exponential terms to zero, which gives $\widetilde{D}_Q^2(R) = 4R^2\sigma^2 + 2N\sigma^4 + NA^2/2$. This corresponds to the variance of a sphere under constant noise $\sigma_\epsilon^2 = NA^2/2$. Intuitively speaking, as the ES approaches a large number of local attractors, its selection is disturbed in a similar way as it is on the noisy sphere. In this case, the variance can be approximated accordingly.

Inserting $\widetilde{D}_Q(R)$ into progress rate (13) and SAR (33), the simplified model is tested in Fig 4 (left). It approximates the σ^*-dip reasonably well. For the derivation of σ^*_{crit} one demands $\varphi_R^{\mathrm{II},*} = 0$ at $R = R_\infty$. Starting from (13) one sets $\varphi_R^{\mathrm{II},*} = \varphi_R^{\mathrm{II}} N/(2R^2)$, $\sigma = \sigma^* R/N$, and uses $\widetilde{D}_Q(R)$, such that after rearranging one obtains the expression

$$1 + \frac{\alpha^2 A}{2} \mathrm{e}^{-\frac{\alpha^2 A N^{3/2}}{\sqrt{128} c_\vartheta \mu} \left(\frac{\sigma^{*2}}{N^2} + \frac{1}{N} \right)} = \sqrt{1 + \frac{\sigma^{*2}}{4c_\vartheta^2 \mu^2} + \frac{\sigma^{*4}}{8Nc_\vartheta^2 \mu^2}}. \tag{37}$$

Solving (37) for σ^* requires further simplifications. As $0 < \sigma^* < \sigma^*_{\varphi_0}$ and $\sigma^*_{\varphi_0} \simeq (8N)^{1/4} (c_\vartheta \mu)^{1/2}$ (see supplementary material B-D), one may assume $\sigma^* = \gamma \sigma^*_{\varphi_0}$ ($0 < \gamma < 1$). Then, one has $\sigma^{*2}/(4c_\vartheta^2 \mu^2) = O(\gamma^2 \sqrt{N}/\mu)$ and $\sigma^{*4}/(8Nc_\vartheta^2 \mu^2) = O(\gamma^4)$. Therefore, the second order term is neglected compared to the fourth order term in (37) for large $\mu \gg \sqrt{N}$. Furthermore, the square-root is expanded using $\sqrt{1+x} = 1 + x/2 + O(x^2)$ and the term $1/N$ in the exponential function can be dropped compared to σ^{*2}/N^2. Finally, one obtains the simplified expression

$$8\alpha^2 A N c_\vartheta^2 \mu^2 \mathrm{e}^{-\frac{\alpha^2 A \sigma^{*2}}{\sqrt{128} N c_\vartheta \mu}} = \sigma^{*4}. \tag{38}$$

Equation (38) can be solved in terms of the Lambert W-function [17] (principal branch denoted as W_0). For $x > 0$ and $y > 0$, it holds

$$x = y\mathrm{e}^y, \quad \text{with inverse function} \quad W_0(x) = y. \tag{39}$$

Introducing $a \coloneqq 8\alpha^2 A N c_\vartheta^2 \mu^2$ and $b \coloneqq \frac{\alpha^2 A}{\sqrt{128} N c_\vartheta \mu}$ in (38), simple manipulations yield $x = a^{1/2} b/2$ and $y = b\sigma^{*2}/2$, such that one solves (38) as

$$\sigma^*_{\mathrm{crit}} = \frac{(512N)^{1/4} (c_\vartheta \mu)^{1/2}}{\alpha A^{1/2}} \sqrt{W_0\left(\frac{\alpha^3 A^{3/2}}{8} \right)}. \tag{40}$$

An exemplary evaluation of (40) is shown in Fig. 4 (right, marked as $*$). Additional parameter variations can be found in the supplementary material B-D. The experiments show good agreement of numerically obtained σ^*_{crit} compared to (40), especially for increasing μ given constant N and A. Setting $\sigma^*_{\mathrm{ss}} = \sigma^*_{\mathrm{crit}}$ and inserting (40) into (35), one obtains

$$\begin{aligned} \tau^2 &= \frac{1}{N} \frac{\frac{8c_\vartheta \sqrt{2N}}{\alpha^2 A} W_0\left(\frac{\alpha^3 A^{3/2}}{8} \right) - c_\vartheta \sqrt{2N}}{1/2 - c_\vartheta \sqrt{2N} + 2e_\vartheta^{1,1}} \\ &= \frac{1}{N} \frac{1 - \frac{8}{\alpha^2 A} W_0\left(\frac{\alpha^3 A^{3/2}}{8} \right)}{1 - 1/(2c_\vartheta \sqrt{2N}) - 2e_\vartheta^{1,1}/(c_\vartheta \sqrt{2N})}. \end{aligned} \tag{41}$$

By neglecting $O(1/\sqrt{N})$ in the denominator of (41), one obtains the result

$$\tau(N, \alpha, A) \simeq \sqrt{\frac{1}{N} \left(1 - \frac{8}{\alpha^2 A} W_0\left(\frac{\alpha^3 A^{3/2}}{8} \right) \right)}. \tag{42}$$

$\tau(N, \alpha, A)$ is real-valued for $\alpha\sqrt{A}/2 > 1.47$ and the limit $\alpha^2 A \to \infty$ of (42) can be easily evaluated as $\tau \simeq 1/\sqrt{N}$ (see supplementary material B-E). This result is interesting since it suggests choosing a larger τ compared to default $\tau = 1/\sqrt{2N}$ in the limit of high multimodality. Choosing a larger τ yields a less robust but faster search, showing (usually) smaller success rates P_S. This observation can be regarded as problematic. To obtain a more complete picture, the efficiency of the ES has to be investigated.

In Figure 5 result (42) is compared to asymptotic $\tau = 1/\sqrt{N}$ and very small $\tau = 1/\sqrt{8N}$ for two different configurations. The sphere steady-state σ^*_{ss} ($R \to \infty, R \to 0$), which is realized by choosing τ via (42), indeed approaches the region of σ^*_{crit} for both configurations. Deviations are expected to occur to some degree as many approximation steps were necessary. The ES moves around the critical point to increase its progress. As expected, $\tau = 1/\sqrt{8N}$ yields a very high P_S-value, but requires a large (mean) number of generations $\overline{g}$ to reach the stopping criterion. $\tau(N, \alpha, A)$ yields a high P_S with good efficiency in terms of $\overline{g}$. Value $\tau = 1/\sqrt{N}$ is less stable and yields $P_S = 0$ (left) and a high value $P_S = 0.94$ (right). However, these experiments were done at fixed population sizes. In the next section, the efficiency is investigated by varying learning parameter τ and population parameters λ and ϑ.

VI. Expected Runtime Experiments

In the previous sections the self-adaptive ES was analyzed by evaluating the progress rate and the self-adaptation response. The theoretical investigations have limitations since the underlying models require the limit $\tau \to 0$. Furthermore, multiple approximation steps were necessary to provide closed-form solutions for $\tau(N, \alpha, A)$ at all. This section should complement the previous results by experimentally evaluating the performance of Alg. 1. To this end, the test function parameters A, α, and N will be fixed, and the strategy parameters λ, τ, and ϑ will be varied over a larger range. Furthermore, restarts of Alg. 1 are introduced and the efficiency is measured in terms of necessary functions evaluations to reach global

This article has been accepted for publication in IEEE Transactions on Evolutionary Computation. This is the author's version which has not been fully edited and content may change prior to final publication. Citation information: DOI 10.1109/TEVC.2024.3400857

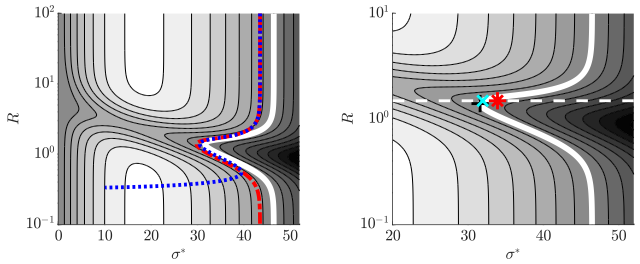

Fig. 4: Plots show configuration of Fig. 2 ($A = 1$). Left plot shows R-iteration using regular variance (14) (dash-dotted red) and simplified variance by setting exponentials to zero (dotted blue). The right plot shows a zoomed-in view with R_∞ (dashed white) and σ^*_{crit} marked (numeric: $+$; $\varphi_R^{\text{II},*}(R_\infty) = 0$: $\times$; result (40): $*$).

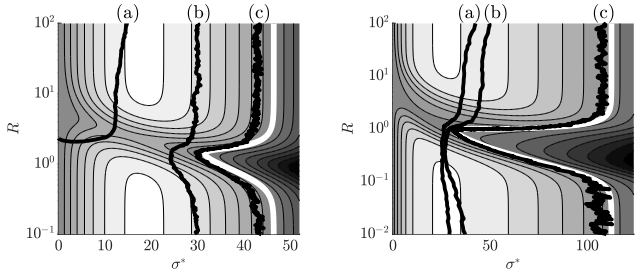

Fig. 5: Left side shows $(100/100_I, 200)$-ES, $N = 100$, $A = 1$, and right side $(500/500_I, 2000)$-ES, $N = 50$, $A = 10$. Both plots show the median over 100 ES-runs with $\tau = 1/\sqrt{N}$ (a), $\tau(N, \alpha, A)$ (b), and $1/\sqrt{8N}$ (c). Success rate P_S and mean number of generations $\overline{g}$ to reach $R = 10^{-4}$ are left ($P_S = 0, 0.92, 0.99$; $\overline{g} = -, 490, 1491$), and right ($P_S = 0.94, 0.97, 1$; $\overline{g} = 175, 185, 1041$). The median is taken over all successful runs (if existing), otherwise over all unsuccessful runs.

convergence. To this end, the expected runtime is evaluated. It was derived in [18] and yields

$$E_r = \left(\frac{1}{P_S} - 1\right)\frac{F_u}{n_u} + \frac{F_s}{n_s} = \frac{F_u + F_s}{n_s}, \tag{43}$$

with the number of total successful and unsuccessful function evaluations denoted as F_s, F_u, respectively, and the number of successful and unsuccessful trials as n_s and n_u, respectively.

For the subsequent experiments, moderately large test function parameters $A = 10$, $\alpha = 2\pi$, and $N = 50$ were chosen. The varied strategy parameters are $\lambda = 200, 400, ..., 2000$, $\tau = 0.05, 0.07, ..., 0.17$, and $\vartheta = 0.1, 0.2, ..., 0.7$, resulting in 490 configurations. Each configuration is evaluated using 200 trials, such that P_S and E_r can be estimated. An overall budget of function evaluations is set to 10^7 (based on configuration $\lambda = 2000$, $\vartheta = 0.5$, $\tau = 0.05$ requiring $E_r \approx 3.3 \cdot 10^6$, plus added headroom). The initialization and termination of each run is based on the following argumentation. One wants to assess the efficiency on the Rastrigin problem by covering the complete landscape of local attraction, but it is desirable to reduce the effects of optimizing the sphere. Therefore, one sets $\mathbf{y}^{(0)} = 30 \cdot \mathbf{1}$ and $\sigma^{(0)} = \sigma^*_{\varphi_0}\|\mathbf{y}\|/N$. This initializes the ES at the beginning of the local attraction region (for $A = 10$). The comparably large $\sigma^{(0)}$ reduces the influence of the initial $\mathbf{y}^{(0)}$. For the termination of successful runs, one sets $f_{\text{stop}} = 10^{-1}$ for the ES being in the global attractor as its closest neighboring local attractor corresponds to $f \approx 1$. This prevents overvaluation of the ES optimizing the sphere limits. Unsuccessful runs terminate below $\sigma_{\text{stop}} = 10^{-3}$ (local convergence) or by reaching the maximum number of function evaluations.

Exemplary evaluations of the experiments are shown in Fig. 6, displaying the success rate and the expected runtime. Contour lines indicate levels of equal P_S and $\log_{10}(E_r)$, see legend at the top. Regions where $P_S = 0$ yield no E_r-value (white regions without data). Note that the contour plots use interpolation between the discrete data points, which improves the visual interpretability.

In general, the highest P_S-values are obtained for large λ and small τ, which was expected. However, these values do not necessarily correspond to the lowest E_r. As an example, in Fig. 6a (top), one obtains the lowest E_r at $\tau \in [0.11, 0.15]$. The notable τ-values are $1/\sqrt{N} \approx 0.14$, $\tau(N, \alpha, A) \approx 0.13$, $1/\sqrt{2N} = 0.1$, and $1/\sqrt{8N} = 0.05$. Choosing $\tau(N, \alpha, A)$ agrees well with the region of lowest E_r. The ES does benefit from approaching the region of σ^*_{crit}, resulting in a better efficiency. One observes that E_r deteriorates as τ decreases. For very large τ-values the σ-adaptation becomes faster and more unstable, such that for some data points no E_r is obtained. Note that a minimum population $\lambda = 400$ is needed to obtain results at all, while for larger $\lambda \geq 800$ E_r does not change much for given τ.

Figures 6b shows the effect of the truncation ratio ϑ given τ. Ratios $\vartheta \in [0.2, 0.5]$ yield satisfying results, which agrees well with standard values $\vartheta = 0.25$ (close to sphere optimal, see [7, Sec. 6.3]) and $\vartheta = 0.5$ (e.g. used for the CMA-ES [19]). Values $\vartheta = \{0.1, 0.6\}$ do work, but they are usually less efficient. $\vartheta = 0.7$ does not yield E_r-results within the given budget of function evaluations. Note that configuration $\vartheta = 0.5$ with $\tau = 0.05$ is relatively inefficient, but yields high P_S. For a single optimization run, it can be recommended due to its robustness. However, its E_r-performance can be improved by either decreasing ϑ or increasing τ. One may conclude that τ and ϑ should not both be chosen too conservatively. Having small τ and large ϑ, the overall convergence rate is significantly reduced. This results in more function evaluations necessary for global convergence.

Figure 6c shows the variation of τ and ϑ for fixed λ. As mentioned before, $\tau = 0.05$ is less efficient. The default value $\tau = 1/\sqrt{2N} = 0.10$ shows better results. However, it should be noted that $\tau = 1/\sqrt{2N}$ was derived in [12] assuming $N \to \infty$ and $\mu \ll N$, which is clearly violated in this experiment. The choice $\tau(N, \alpha, A) \approx 0.13$ using (42) yields very good results in terms of E_r. One observes that even larger $1/\sqrt{N} \approx 0.14$ yields good results (provided that λ is large enough).

The results of a second experiment at $N = 200$, $A = 1$, and $\alpha = 2\pi$ are comparable to Fig. 6 and are given in the supplementary material B-F.

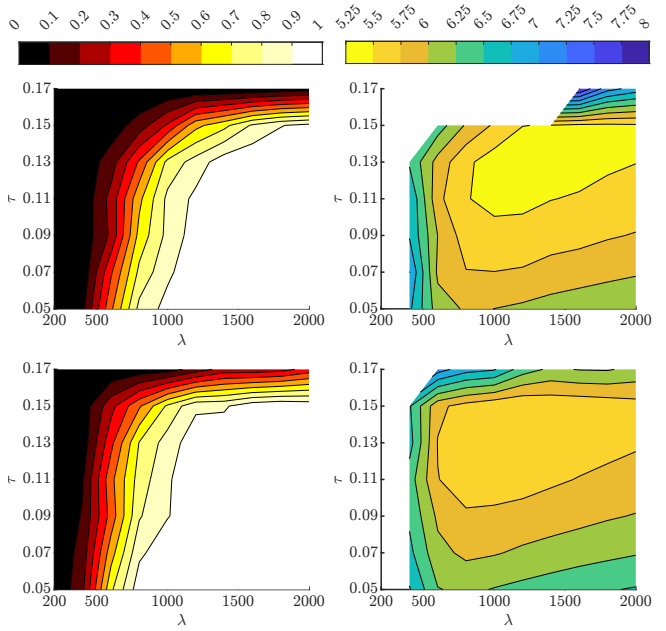

(a) Variation of λ (x-axis) and τ (y-axis) for $\vartheta = 0.3$ (top) and $\vartheta = 0.5$ (bottom).

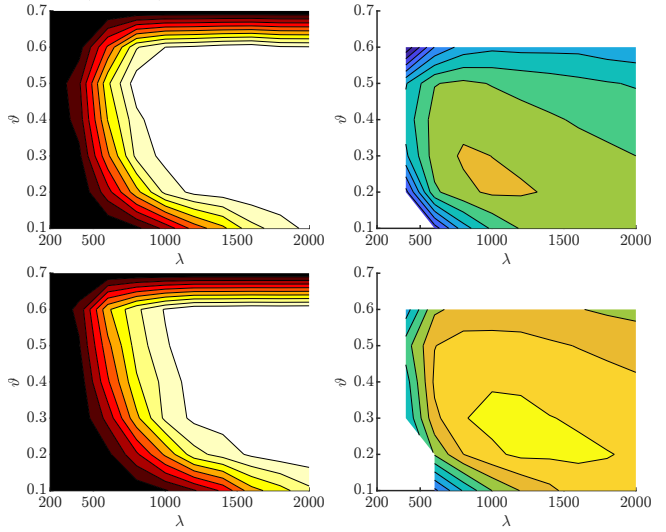

(b) Variation of λ (x-axis) and ϑ (y-axis) for $\tau = 0.05$ (top) and $\tau = 0.11$ (bottom).

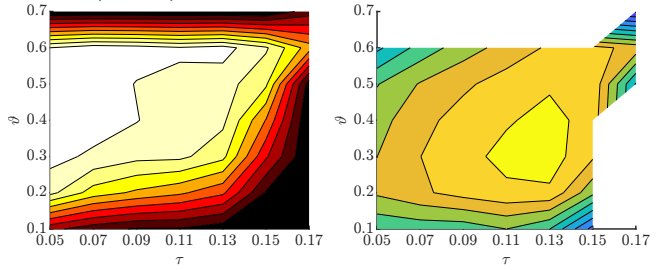

(c) Variation of τ (x-axis) and ϑ (y-axis) for $\lambda = 1000$.

Fig. 6: Variation of λ, τ, and ϑ at $A = 10$ and $N = 50$. The left column shows the success rate P_S and the right column $\log_{10}(E_r)$, see (43). The legend is placed at the top.

VII. Conclusion and Outlook

In this paper, an asymptotically exact self-adaptation response (SAR) function was derived in (31) for large populations and small learning parameter τ. Subsequently, it was evaluated on the highly multimodal Rastrigin function. Within a dynamic model of the self-adaptive ES, progress rate and SAR results were used to investigate the convergence and steady-state properties of the ES as a function of the learning parameter τ. On Rastrigin, the normalized mutation strength σ^* is dependent on the residual distance R, which is in contrast to the sphere function (where a constant steady-state σ^* exists). Due to local attraction, one observes a characteristic decrease of σ^*. Local attraction demands σ^* fall below a critical value σ^*_{crit}. By investigating σ^*_{crit} an approximate model thereof could be derived. Demanding that the self-adaptation reaches its (sphere) steady-state at σ^*_{crit}, the learning parameter dependency $\tau(N, \alpha, A)$ could be derived for Rastrigin.

Expected runtime experiments show that $\tau(N, \alpha, A)$ does not maximize the success rate P_S compared to smaller choices of τ. Instead, it shows a higher efficiency of the search in terms of function evaluations. Therefore, comparably large $\tau \in [1/\sqrt{2N}, 1/\sqrt{N}]$ may be beneficial on multimodal functions, if restarts are allowed and the population size is sufficiently large. Whether this observation holds for other multimodal test functions with adequate global structure is an open question. On the other hand, the highest robustness (at the expense of efficiency) is achieved for small τ, high ϑ, and large populations, which was expected. Whether and how the results could be transferred to cumulative step-size adaptation (CSA) is left for future research.

A general important observation is that minimal population sizes are needed to obtain global convergence at all (see also [3]). For black-box optimization problems there is no knowledge about the degree of multimodality, e.g., parameters α and A, to tune the ES appropriately. Furthermore, allowing algorithm restarts opens up the question of how to re-initialize the ES-parameters. Therefore, adaptive population control appears to be a natural direction for future research.

References

[1] H.-G. Beyer and H.-P. Schwefel, "Evolution Strategies: A Comprehensive Introduction," *Natural Computing*, vol. 1, no. 1, pp. 3–52, 2002.

[2] N. Hansen and S. Kern, "Evaluating the CMA Evolution Strategy on Multimodal Test Functions," in *Parallel Problem Solving from Nature 8*, X. Yao et al., Ed. Berlin: Springer, 2004, pp. 282–291.

[3] L. Schönenberger and H.-G. Beyer, "On a Population Sizing Model for Evolution Strategies Optimizing the Highly Multimodal Rastrigin Function," in *Proceedings of the Genetic and Evolutionary Computation Conference*, ser. GECCO '23, New York, NY, USA, 2023, p. 848–855. [Online]. Available: https://doi.org/10.1145/3583131.3590451

[4] A. Omeradzic and H.-G. Beyer, "Convergence Properties of the $(\mu/\mu_I, \lambda)$-ES on the Rastrigin Function," in *Proceedings of the 17th ACM/SIGEVO Conference on Foundations of Genetic Algorithms*, ser. FOGA '23. New York, NY, USA: Association for Computing Machinery, 2023, p. 117–128. [Online]. Available: https://doi.org/10.1145/3594805.3607126

[5] I. Rechenberg, *Evolutionsstrategie: Optimierung technischer Systeme nach Prinzipien der biologischen Evolution*. Stuttgart: Frommann-Holzboog Verlag, 1973.

[6] H.-P. Schwefel, *Numerische Optimierung von Computer-Modellen mittels der Evolutionsstrategie*, ser. Interdisciplinary systems research; 26. Basel: Birkhäuser, 1977.

[7] H.-G. Beyer, *The Theory of Evolution Strategies*, ser. Natural Computing Series. Heidelberg: Springer, 2001, DOI: 10.1007/978-3-662-04378-3.

[8] A. Ostermeier, "Schrittweitenadaptation in der Evolutionsstrategie mit einem entstochastisierten Ansatz," Doctoral thesis, Technical University of Berlin, Berlin, 1997.

[9] N. Hansen and A. Ostermeier, "Completely Derandomized Self-Adaptation in Evolution Strategies," *Evolutionary Computation*, vol. 9, no. 2, pp. 159–195, 2001, https://doi.org/10.1162/106365601750190398.

[10] N. Hansen, A. Auger, R. Ros, O. Mersmann, T. Tušar, and D. Brockhoff, "COCO: A platform for comparing continuous optimizers in a black-box setting," *Optimization Methods and Software*, vol. 36, pp. 114–144, 2021.

[11] N. Hansen, A. Auger, R. Ros, S. Finck, and P. Pošík, "Comparing Results of 31 Algorithms from the Black-Box Optimization Benchmarking BBOB-2009," in *Proceedings of the 12th Annual Conference Companion on Genetic and Evolutionary Computation*, ser. GECCO '10. New York, NY, USA: Association for Computing Machinery, 2010, p. 1689–1696. [Online]. Available: https://doi.org/10.1145/1830761.1830790

[12] S. Meyer-Nieberg, "Self-Adaptation in Evolution Strategies," Ph.D. dissertation, University of Dortmund, CS Department, Dortmund, Germany, 2007.

[13] H.-G. Beyer and A. Melkozerov, "The Dynamics of Self-Adaptive Multi-Recombinant Evolution Strategies on the General Ellipsoid Model," *IEEE Transactions on Evolutionary Computation*, vol. 18, no. 5, pp. 764–778, 2014, DOI: 10.1109/TEVC.2013.2283968.

[14] H.-P. Schwefel, *Numerical Optimization of Computer Models*. Chichester: Wiley, 1981.

[15] A. Omeradzic and H.-G. Beyer, "Progress Analysis of a Multi-Recombinative Evolution Strategy on the Highly Multimodal Rastrigin Function," *Theoretical Computer Science*, vol. 978, 2023. [Online]. Available: https://doi.org/10.1016/j.tcs.2023.114179

[16] D. Arnold, *Noisy Optimization with Evolution Strategies*. Dordrecht: Kluwer Academic Publishers, 2002.

[17] F. Olver, D. Lozier, R. Boisvert, and C. Clark, *The NIST Handbook of Mathematical Functions*. Cambridge University Press, New York, NY, 2010.

[18] A. Auger and N. Hansen, "Performance Evaluation of an Advanced Local Search Evolutionary Algorithm," in *Congress on Evolutionary Computation, CEC'05*, vol. 2. IEEE, 2005, pp. 1777–1784.

[19] N. Hansen, "The CMA Evolution Strategy: A Tutorial," 2023.

[20] A. Hoorfar and M. Hassani, "Inequalities on the Lambert function and hyperpower function," *JIPAM. Journal of Inequalities in Pure & Applied Mathematics [electronic only]*, vol. 9, 2008. [Online]. Available: http://eudml.org/doc/130024

Amir Omeradzic received his Bachelor's and Master's degree in Computational Physics from ETH Zurich, Switzerland. Currently, he is a research associate in the field of evolutionary computation at the Vorarlberg University of Applied Sciences, Austria, and pursues his Ph.D. in computer science at the Ulm University, Germany. His research interests include evolutionary algorithms, neural networks, statistical physics, and their applications in real-world problems.

Hans-Georg Beyer received the Diploma degree in Theoretical Electrical Engineering from the Ilmenau Technical University, Germany, in 1982 and the Ph.D. in physics from Bauhaus-University Weimar, Weimar, Germany, in 1989, and the Habilitation degree in computer science from the University of Dortmund, Dortmund, Germany, in 1997. Since 2004 he has been professor with the Vorarlberg University of Applied Sciences, Dornbirn, Austria. He authored the book "The Theory of Evolution Strategies" (Heidelberg: Springer-Verlag, 2001) and authored/coauthored numerous papers in that field. Dr. Beyer was the Editor-in-Chief of the MIT Press Journal "Evolutionary Computation" and served as an Associate Editor for the IEEE "Transactions on Evolutionary Computation" from 1997 to 2021.

APPENDIX A
SELF-ADAPTATION RESPONSE

Starting from (30) the order statistic density $p_{m;\lambda}(s|\sigma)$ needs to be derived. An offspring samples its mutation strength according to density $p_\sigma(s)$ in (29). Furthermore, a quality gain q is observed with conditional density $p_Q(q|s)$ and CDF $P_Q(q|s)$. The conditional CDF of the quality gain given σ for an individual sampling mutations from $p_\sigma(s)$ is obtained by

$$P_{Q,s}(q|\sigma) = \int_0^\infty P_Q(q|s)p_\sigma(s)\,\mathrm{d}s\,. \tag{A.1}$$

For the m-th best individual having quality gain q, there are $m-1$ better and $\lambda - m$ worse individuals, respectively. The order statistic density for the m-th best individual given σ is obtained by integration over all quality gain values using (A.1)

$$p_{m;\lambda}(s|\sigma) = p_\sigma(s)\frac{\lambda!}{(m-1)!(\lambda-m)!}\int_{q_l}^{q_u} p_Q(q|s) \times P_{Q,s}(q|\sigma)^{m-1}(1-P_{Q,s}(q|\sigma))^{\lambda-m}\,\mathrm{d}q\,. \tag{A.2}$$

For log-normal mutations (29) and a normally distributed quality gain (7), a closed-form solution of Eq. (A.1) cannot be provided. However, for small learning parameter τ it will be shown by the same argumentation as in Eqs. (A.15) and (A.16) that

$$P_{Q,s}(q|\sigma) = P_Q(q|\sigma) + O\left(\tau^2\right). \tag{A.3}$$

Inserting (A.3) into (A.2), and the result into (30), one gets by neglecting higher orders of τ and exchanging the sum and integral

$$\psi = \int_0^\infty \left(\frac{s-\sigma}{\sigma}\right)p_\sigma(s)\frac{\lambda!}{\mu}\int_{q_l}^{q_u} p_Q(q|s) \times \sum_{m=1}^{\mu}\frac{P_Q(q|\sigma)^{m-1}(1-P_Q(q|\sigma))^{\lambda-m}}{(m-1)!(\lambda-m)!}\,\mathrm{d}q\,\mathrm{d}s\,. \tag{A.4}$$

Given (A.4) the following identity from [7, (5.14)] is applied

$$\sum_{m=1}^{\mu}\frac{P(q)^{m-1}[1-P(q)]^{\lambda-m}}{(m-1)!(\lambda-m)!} = \frac{1}{(\lambda-\mu-1)!(\mu-1)!}\int_0^{1-P(q)} t^{\lambda-\mu-1}(1-t)^{\mu-1}\,\mathrm{d}t\,, \tag{A.5}$$

such that (A.4) yields by using (A.5)

$$\psi = \int_0^\infty \left(\frac{s-\sigma}{\sigma}\right)p_\sigma(s)\frac{\lambda!}{(\lambda-\mu-1)!\mu!}\int_{q_l}^{q_u} p_Q(q|s) \times \int_0^{1-P_Q(q|\sigma)} t^{\lambda-\mu-1}(1-t)^{\mu-1}\,\mathrm{d}t\,\mathrm{d}q\,\mathrm{d}s\,. \tag{A.6}$$

The population dependent factor in (A.6) is rewritten in terms of the beta function B and truncation ratio $\vartheta = \mu/\lambda$ as $\frac{\lambda!}{(\lambda-\mu-1)!\mu!} = \frac{1}{\vartheta}\frac{1}{\mathrm{B}(\lambda-\mu,\mu)}$. Furthermore, one can exchange the integral bounds $q_l \le q \le q_u$, and $0 \le t \le 1 - P_Q(q|\sigma)$ by applying the inverse CDF P_Q^{-1} to $q = P_Q^{-1}(1-t)$ giving

$0 \leq t \leq 1, \quad \text{and} \quad q_l \leq q \leq P_Q^{-1}(1-t|\sigma)$. Refactoring and exchanging the bounds in (A.6), one gets

$$\psi = \frac{1}{\vartheta}\int_0^\infty \left(\frac{s-\sigma}{\sigma}\right)\frac{p_\sigma(s)}{\mathrm{B}(\lambda-\mu,\mu)}\int_0^1 t^{\lambda-\mu-1}(1-t)^{\mu-1} \times \int_{q_l}^{P_Q^{-1}(1-t|\sigma)} p_Q(q|s)\,\mathrm{d}q\,\mathrm{d}t\,\mathrm{d}s\,. \quad \text{(A.7)}$$

The innermost integration over q can be easily evaluated as

$$\int_{q_l}^{P_Q^{-1}(1-t|\sigma)} p_Q(q|s)\,\mathrm{d}q = P_Q\Big(P_Q^{-1}(1-t|\sigma)\Big|s\Big), \quad \text{(A.8)}$$

where the probability $P_Q(q_l|s) = \Pr(Q \leq q_l|s) = 0$ for any lower bound value q_l. Inserting (A.8) into (A.7) yields

$$\psi = \frac{1}{\vartheta}\int_0^\infty \left(\frac{s-\sigma}{\sigma}\right)\frac{p_\sigma(s)}{\mathrm{B}(\lambda-\mu,\mu)}\int_0^1 t^{\lambda-\mu-1}(1-t)^{\mu-1} \times P_Q\Big(P_Q^{-1}(1-t|\sigma)\Big|s\Big)\,\mathrm{d}t\,\mathrm{d}s\,. \quad \text{(A.9)}$$

The t-integral in (A.9) is now evaluated in the limit $\mu, \lambda \to \infty$ ($\vartheta = \mu/\lambda$) by applying the same method as in the proof of [15, Theorem 1] using the dominated convergence theorem. One can define a sequence $g_\mu := \frac{1}{\mathrm{B}(\lambda-\mu,\mu)}\int_0^1 t^{\lambda-\mu-1}(1-t)^{\mu-a} f_{\sigma,s}(t)\,\mathrm{d}t$ for $a = 1$, $\mu > a$ and $\lambda(\mu) = \mu/\vartheta$ with $f_{\sigma,s}(t)$ defined for constant values of $\sigma, s \geq 0$ and $0 \leq f_{\sigma,s}(t) \leq 1$. It can be shown that $|g_\mu(x)| \leq 1$ using [15, Eq. (43)]. Furthermore, the s-integral in (A.9) is finite with $\mathrm{E}\left[\frac{s-\sigma}{\sigma}\right] = \tau^2/2$ using (A.16). Therefore, an upper bound of (A.9) is given by $\tau^2/2\vartheta$, such that limit and s-integral can be exchanged in (A.9). The limit of g_μ yields [15, Eq. (39)] with $f_{\sigma,s} = P_Q(P_Q^{-1}(1-t|\sigma)|s)$

$$\lim_{\substack{\mu,\lambda\to\infty \\ \vartheta=\text{const.}}} g_\mu = f_{\sigma,s}(t)\big|_{t=1-\vartheta} = P_Q\Big(P_Q^{-1}(\vartheta|\sigma)\Big|s\Big), \quad \text{(A.10)}$$

such that the asymptotic equality for the SAR is obtained

$$\psi \simeq \frac{1}{\vartheta}\int_0^\infty \left(\frac{s-\sigma}{\sigma}\right)p_\sigma(s)P_Q\Big(P_Q^{-1}(\vartheta|\sigma)\Big|s\Big)\,\mathrm{d}s\,. \quad \text{(A.11)}$$

Now the actual distribution for P_Q and its inverse for P_Q^{-1} are required to further evaluate (A.11). Using the normal approximation (7), one has

$$P_Q(q|s) \simeq \Phi\left(\frac{q - E_Q(s)}{D_Q(s)}\right) = p, \quad \text{(A.12)}$$

yielding a probability value p. The inverse P_Q^{-1} is obtained using the inverse of the normal distribution $\Phi^{-1}(p)$ given probability p and mutations strength σ

$$q = E_Q(\sigma) + D_Q(\sigma)\Phi^{-1}(p). \quad \text{(A.13)}$$

From now on we use the abbreviations $E(s) := E_Q(s)$, $D(s) := D_Q(s)$ and $\Phi_\vartheta^{-1} := \Phi^{-1}(\vartheta)$ for brevity. Inserting (A.13) into (A.12) and the result into (A.11) yields

$$\psi \simeq \frac{1}{\vartheta}\int_0^\infty \left(\frac{s-\sigma}{\sigma}\right)p_\sigma(s) \times \Phi\left(\frac{E(\sigma) + D(\sigma)\Phi_\vartheta^{-1} - E(s)}{D(s)}\right)\mathrm{d}s\,. \quad \text{(A.14)}$$

A closed-form solution of (A.14) cannot be given as the functional dependencies of $E(s)$, see (8), and $D(s)$, see (9), are too complex. However, for $\tau \to 0$ a solution can be given in terms of a Taylor expansion around σ by neglecting higher order terms of $(\frac{s-\sigma}{\sigma})^k$. In [12, Appendix C.2] it was shown that for $k \geq 3$ one has $\mathrm{E}\left[\left(\frac{s-\sigma}{\sigma}\right)^k\right] = O\left(\tau^4\right)$. Therefore, the expected value of a function f w.r.t. $p_\sigma(s)$ is expanded in terms of factor $\Delta_s^k := (s-\sigma)^k/\sigma^k$ and truncated for $k \geq 3$. Using abbreviation $\partial^k f/\partial s^k\,|_{s=\sigma} =: f_\sigma^{(k)}$, one gets

$$\begin{aligned}
\mathrm{E}\left[f(s)\right] &= \int_0^\infty f(s)p_\sigma(s)\,\mathrm{d}s \\
&= \int_0^\infty \sum_{k=0}^\infty \frac{\sigma^k}{k!}\frac{\partial^k f}{\partial s^k}\bigg|_{s=\sigma}\Delta_s^k p_\sigma(s)\,\mathrm{d}s \\
&= \int_0^\infty \left[f_\sigma^{(0)} + \sigma f_\sigma^{(1)}\Delta_s + \frac{\sigma^2 f_\sigma^{(2)}}{2}\Delta_s^2 + O\big(\Delta_s^3\big)\right]p_\sigma(s)\,\mathrm{d}s \\
&\simeq f_\sigma^{(0)} + \sigma f_\sigma^{(1)}\,\mathrm{E}\left[\Delta_s\right] + \frac{\sigma^2 f_\sigma^{(2)}}{2}\,\mathrm{E}\left[\Delta_s^2\right] + O\left(\tau^4\right).
\end{aligned} \quad \text{(A.15)}$$

Using $\mathrm{E}\left[s^k\right] = \sigma^k \mathrm{e}^{\frac{1}{2}k^2\tau^2}$ for a log-normal variate and expansion $\mathrm{e}^{\frac{1}{2}\tau^2} = 1 + \frac{1}{2}\tau^2 + O\left(\tau^4\right)$, one has

$$\mathrm{E}\left[\Delta_s\right] = \tau^2/2 + O\left(\tau^4\right), \quad \mathrm{E}\left[\Delta_s^2\right] = \tau^2 + O\left(\tau^4\right). \quad \text{(A.16)}$$

In (A.3) only the zeroth order term of (A.15) is used to simplify the CDF neglecting $O\left(\tau^2\right)$. Expression (A.14) already contains Δ_s, such that for $O\left(\tau^4\right)$ one needs to evaluate $f_\sigma^{(0)}$ and $f_\sigma^{(1)}$ using for $f(s) = \Phi(\dots)$. One obtains by denoting the derivative w.r.t. σ with prime symbol $'$

$$\begin{aligned}
f_\sigma^{(0)} &= \Phi\left(\frac{E(\sigma) + D(\sigma)\Phi_\vartheta^{-1} - E(\sigma)}{D(\sigma)}\right) = \vartheta \\
f_\sigma^{(1)} &= \frac{\partial f}{\partial s}\bigg|_{s=\sigma} = -\frac{\mathrm{e}^{-\frac{1}{2}[\Phi_\vartheta^{-1}]^2}}{\sqrt{2\pi}}\frac{E'(\sigma) + \Phi_\vartheta^{-1}D'(\sigma)}{D(\sigma)}.
\end{aligned} \quad \text{(A.17)}$$

Using (A.16) and (A.17) in (A.15), and dropping $O\left(\tau^4\right)$-terms, the SAR yields

$$\begin{aligned}
\psi &\simeq \frac{1}{\vartheta}\left(\vartheta\frac{1}{2}\tau^2 - \sigma\frac{1}{\sqrt{2\pi}}\mathrm{e}^{-\frac{1}{2}[\Phi_\vartheta^{-1}]^2}\frac{E'(\sigma) + \Phi_\vartheta^{-1}D'(\sigma)}{D(\sigma)}\tau^2\right) \\
&= \tau^2\left[\frac{1}{2} - \sigma\frac{\mathrm{e}^{-\frac{1}{2}[\Phi_\vartheta^{-1}]^2}}{\sqrt{2\pi}\vartheta}\frac{E'(\sigma)}{D(\sigma)} - \sigma\frac{\Phi_\vartheta^{-1}}{\sqrt{2\pi}\vartheta}\mathrm{e}^{-\frac{1}{2}[\Phi_\vartheta^{-1}]^2}\frac{D'(\sigma)}{D(\sigma)}\right].
\end{aligned} \quad \text{(A.18)}$$

In (A.18) the asymptotic generalized progress coefficient $e_\vartheta^{a,b}$ can be recognized from (11) as

$$e_\vartheta^{1,0} = c_\vartheta = \frac{\mathrm{e}^{-\frac{1}{2}[\Phi_\vartheta^{-1}]^2}}{\sqrt{2\pi}\vartheta}, \quad e_\vartheta^{1,1} = -\frac{\Phi_\vartheta^{-1}\mathrm{e}^{-\frac{1}{2}[\Phi_\vartheta^{-1}]^2}}{\sqrt{2\pi}\vartheta}. \quad \text{(A.19)}$$

We finally arrive at the SAR in the limit of $N \to \infty$, $\tau \to 0$, and $(\mu, \lambda) \to \infty$ (constant $\vartheta = \mu/\lambda$) as

$$\psi \simeq \tau^2\left(\frac{1}{2} - c_\vartheta\sigma\frac{E_Q'(\sigma)}{D_Q(\sigma)} + e_\vartheta^{1,1}\sigma\frac{D_Q'(\sigma)}{D_Q(\sigma)}\right). \quad \text{(A.20)}$$

APPENDIX B
SUPPLEMENTARY MATERIAL

Symbol	Description
σ	mutation strength
τ	learning parameter (self-adaptation)
f	Rastrigin test function
$\mathbf{y}$	search vector
N	dimensionality
A	Rastrigin oscillation amplitude
α	Rastrigin oscillation frequency
R	residual distance
g	generation counter
μ	parent population size
λ	offspring population size
ϑ	selection ratio μ/λ
φ_i	first-order component-wise progress rate
φ_i^{II}	second-order component-wise progress rate
φ_R^{II}	R-dependent progress rate
ψ	self-adaptation response function
Q	local quality gain
Φ	standard normal distribution function
Φ^{-1}	inverse of Φ (quantile function)
E_Q	expected value of Q
D_Q^2	variance of Q
$c_\vartheta, e_\vartheta^{1,1}$	asymptotic progress coefficients
σ^*	normalized mutation strength
$\sigma^*_{\varphi_0}$	second-zero of sphere progress rate
$\varphi_R^{\mathrm{II},*}$	normalized R-dependent progress rate
σ^*_{ss}	steady-state σ^*
P_S	success rate of global convergence
σ^*_{crit}	critical σ^*
R_∞	residual distance under constant noise
W_0	Lambert W-function
E_r	expected runtime

TABLE I: List of symbols sorted by their first occurrence.

A. Expected Value of Quality Gain

The expected value of the quality gain $Q = f(\mathbf{y}+\mathbf{x}) - f(\mathbf{y})$, see (6), at location $\mathbf{y}$ due to a random mutation $\mathbf{x} \sim \sigma\mathcal{N}(\mathbf{0},\mathbf{1})$, was already derived in [15, (30)] as

$$E_Q(\mathbf{y}) = \sum_{i=1}^{N}\left[\sigma^2 + A\cos(\alpha y_i)\left(1-\mathrm{e}^{-\frac{(\alpha\sigma)^2}{2}}\right)\right]. \quad \text{(B.1)}$$

The goal is to derive the aggregated (averaged) value $E_Q(R)$, given (B.1) with $R^2 = \sum_i y_i^2$. The approach developed in [4] is followed. It is assumed that the ES performs a global search with $y_i \sim \mathcal{N}(0, R^2/N)$, see (12), such that stochastic averaging can be applied. The first term of (B.1) is independent of y_i and the summation is straightforward, which gives

$$E_Q(\mathbf{y}) = N\sigma^2 + A\Big(1-\mathrm{e}^{-\frac{(\alpha\sigma)^2}{2}}\Big)\sum_{i=1}^{N}\cos(\alpha y_i) \quad \text{(B.2)}$$

For the second term, one defines for the sum over the cosine terms

$$Y \coloneqq \sum_{i=1}^{N}\cos(\alpha y_i). \quad \text{(B.3)}$$

The terms in (B.3) are independent and identically distributed. Applying the Central Limit Theorem in the limit $N\to\infty$, the sum approaches a normal distribution with $Y \sim \mathrm{E}[Y] + \sqrt{\mathrm{Var}[Y]}\mathcal{N}(0,1)$. In [4, (A.7)] it was shown that

$$\sqrt{\mathrm{Var}[Y]}/\mathrm{E}[Y] \overset{N\to\infty}{\longrightarrow} 0, \quad \text{(B.4)}$$

where the ratio of (B.4) vanishes as $O(1/\sqrt{N})$. In the limit $N\to\infty$ one can neglect the fluctuations of the random variate Y. Hence, it is replaced by its expected value $Y \simeq \mathrm{E}[Y]$. Thus, the average $E_Q(R)$ is obtained by taking the expected value over the y_i in (B.2). The expected value over the cosine terms was evaluated in [15, (29)] and yields

$$\mathrm{E}\left[\sum_{i=1}^{N}\cos(\alpha y_i)\right] = N\mathrm{e}^{-\frac{1}{2}\frac{(\alpha R)^2}{N}}. \quad \text{(B.5)}$$

Finally, the aggregated (R-dependent) quality gain expected value yields

$$E_Q(R) = N\sigma^2 + NA\mathrm{e}^{-\frac{1}{2}\frac{(\alpha R)^2}{N}}\Big(1-\mathrm{e}^{-\frac{(\alpha\sigma)^2}{2}}\Big). \quad \text{(B.6)}$$

The same method and argumentation were used in [4] to derive the aggregated (averaged) quality gain variance D_Q^2 in (14).

B. Progress Rate and SAR Landscapes

Figure 7 shows the result of Fig. 3 (left plot, $A=1$) in color. Furthermore, the corresponding SAR is displayed. Bold white lines denote the respective zeros of $\varphi_R^{\mathrm{II},*}$ and ψ. Regions of high progress are shown in yellow, while regions of low (negative) progress are dark blue. As τ is relatively small, the median dynamics of the ES achieves relatively high σ^*-levels. In the sphere limits ($R\to\infty, R\to 0$) one observes σ^* close to $\sigma^*_{\varphi_0} \approx 47$. During the transitional phase, σ^* stays close to the progress dip. In the sphere limits, one observes vertical lines indicating scale-invariant progress rate and SAR. In this limit the sphere steady-state condition (28) is valid and convergence occurs for $\varphi_R^{\mathrm{II},*}(\sigma^*, R) > 0$ and $\psi < 0$ (satisfied in the plot). Along the progress dip, ψ changes significantly as σ^* is reduced to achieve positive progress.

C. Steady-State Condition

Starting from (28), the steady-state condition (35) for the sphere is derived. The progress rate is already given in (17). The SAR on the sphere requires setting $A=0$ in $E_Q(R)$, see (15), and $D_Q^2(R)$, see (14), and evaluating respective derivatives. One gets for the expected value of the sphere (using $\sigma = \sigma^* R/N$)

$$\begin{aligned} E_Q &= N\sigma^2 \\ E'_Q &= \frac{\mathrm{d}E_Q}{\mathrm{d}\sigma} = 2N\sigma = 2N\frac{\sigma^* R}{N}, \end{aligned} \quad \text{(B.7)}$$

and for the variance terms

$$\begin{aligned} D_Q^2 &= 4R^2\sigma^2 + 2N\sigma^4 = 4R^2\left(1+\frac{\sigma^{*2}}{2N}\right) \\ D'_Q &= \frac{\mathrm{d}(D_Q^2)}{\mathrm{d}\sigma}\frac{1}{2D_Q} = \frac{8R^2\sigma + 8N\sigma^3}{2(4\sigma^2R^2 + 2N\sigma^4)^{1/2}} \\ &= \frac{2R\Big(1+\frac{\sigma^{*2}}{N}\Big)}{\sqrt{1+\frac{\sigma^{*2}}{2N}}}. \end{aligned} \quad \text{(B.8)}$$

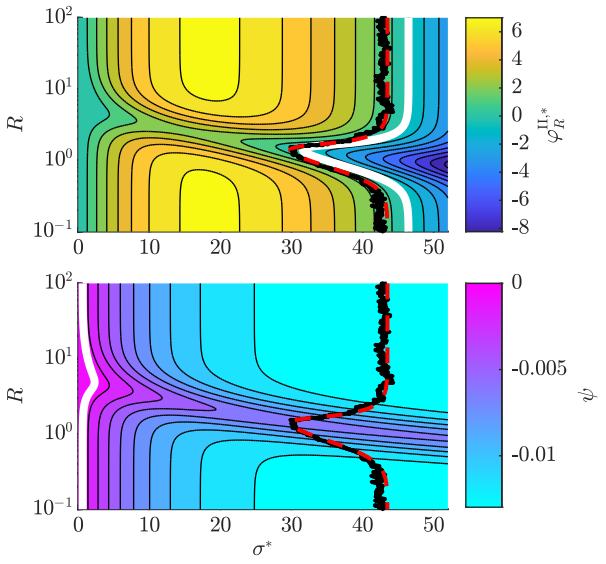

Fig. 7: The top plot shows the progress rate $\varphi_R^{\mathrm{II},*}(\sigma^*, R)$, see Eq. (13), and the bottom plot the SAR function $\psi(\sigma^*, R)$, see (33), for the $(100/100_I, 200)$-ES, $N = 100$, $\tau = 1/\sqrt{8N}$, with overlaid median dynamics of Alg. 1 (black) and iterated dynamics of Eq. (23) (dashed red).

Using (B.7) and (B.8) in SAR-function (31) yields

$$\psi_{\mathrm{sph}}(\sigma^*) = \tau^2 \left(\frac{1}{2} - c_\vartheta \frac{\sigma^*}{\sqrt{1 + \frac{\sigma^{*2}}{2N}}} + e_\vartheta^{1,1} \frac{1 + \frac{\sigma^{*2}}{N}}{1 + \frac{\sigma^{*2}}{2N}} \right). \quad \text{(B.9)}$$

Now one inserts (17) and (B.9) into (28) and sets $\sigma^* = \sigma^*_{ss}$ (steady-state), which gives

$$\frac{c_\vartheta \sigma^*_{\mathrm{ss}}}{\sqrt{1 + \frac{\sigma^{*2}_{\mathrm{ss}}}{2N}}} - \frac{\sigma^{*2}_{\mathrm{ss}}}{2\mu} = -N\tau^2 \left(\frac{1}{2} - \frac{c_\vartheta \sigma^*_{\mathrm{ss}}}{\sqrt{1 + \frac{\sigma^{*2}_{\mathrm{ss}}}{2N}}} + e_\vartheta^{1,1} \frac{1 + \frac{\sigma^{*2}_{\mathrm{ss}}}{N}}{1 + \frac{\sigma^{*2}_{\mathrm{ss}}}{2N}} \right). \quad \text{(B.10)}$$

Condition (B.10) has several important properties.[1] In the limit $N \to \infty$ (small σ^* as $\mu \ll N$), the terms simplify significantly by dropping $O\left(\sigma^{*2}/N\right)$, giving the result $c_\vartheta \sigma^*_{\mathrm{ss}} - \frac{\sigma^{*2}_{\mathrm{ss}}}{2\mu} = -N\tau^2(\frac{1}{2} - c_\vartheta \sigma^*_{\mathrm{ss}} + e_\vartheta^{1,1})$, for which (after replacing c_ϑ by $c_{\mu/\mu,\lambda}$) the default $\tau = 1/\sqrt{2N}$ was derived in [12, Sec. 4.1]. In the case of the Rastrigin function, the assumption of $\mu \ll N$ does not hold as μ must be chosen relatively large to obtain high success rates. Additionally, the choice of a large μ rescales the steady-state σ^*, see scaling of second zero (B.13) w.r.t. μ. Therefore, by assuming $\mu \to \infty$, constant N, and the scaling (B.13), one can simplify the last term of ψ by evaluating $\lim_{\sigma^* \to \infty}(1 + \frac{\sigma^{*2}_{\mathrm{ss}}}{N})/(1 + \frac{\sigma^{*2}_{\mathrm{ss}}}{2N}) = 2$.

[1]For condition (B.10) it should be noted that a closed-form solution for σ^*_{ss} is in principle possible, but due to its very lengthy result practically not usable. The same observation holds for the optimal $\hat{\sigma}^*_{ss}$ maximizing the progress rate in (17), which (technically) can be obtained by evaluating $\frac{\mathrm{d}\varphi^*}{\mathrm{d}\sigma^*} = 0$, but yields very lengthy results.

Furthermore, one has $\sqrt{1 + \sigma^{*2}_{\mathrm{ss}}/2N} \simeq \sigma_{ss}/\sqrt{2N}$. Under these assumptions (B.10) simplifies as

$$c_\vartheta \sqrt{2N} - \frac{\sigma^{*2}_{\mathrm{ss}}}{2\mu} = -N\tau^2 \left(\frac{1}{2} - c_\vartheta \sqrt{2N} + 2e_\vartheta^{1,1} \right). \quad \text{(B.11)}$$

D. Deriving and Evaluating σ^*_{crit}

First, the second zero of the progress rate is simplified. Starting from (19), the second zero for $\mu^2 \gg N$ yields

$$\begin{aligned} \sigma^*_{\varphi_0} &= \left[N \left(1 + \frac{8c_\vartheta^2 \mu^2}{N} \right)^{1/2} - N \right]^{1/2} \\ &\simeq \left[N \left(\frac{8c_\vartheta^2 \mu^2}{N} \right)^{1/2} - N \right]^{1/2} \\ &= \left[(8N)^{1/2} c_\vartheta \mu - N \right]^{1/2} \\ &= (8N)^{1/4} (c_\vartheta \mu)^{1/2} \left[1 - \frac{N}{(8N)^{1/2} c_\vartheta \mu} \right]^{1/2} \\ &= (8N)^{1/4} (c_\vartheta \mu)^{1/2} \left[1 - O\left(\frac{\sqrt{N}}{\mu} \right) \right], \end{aligned} \quad \text{(B.12)}$$

which yields after neglecting $O(\sqrt{N}/\mu)$

$$\sigma^*_{\varphi_0} \simeq (8N)^{1/4} (c_\vartheta \mu)^{1/2}. \quad \text{(B.13)}$$

Equation (B.13) is then used to neglect terms in Eq. (37) and provide a closed-form solution of σ^*_{crit}.

In Fig. 8, experiments regarding σ^*_{crit} from Eq. (40) are conducted. To this end, μ, N, and A are varied, respectively. The numeric solution serves as a reference. Approximation (40) yields comparably good results considering that multiple simplifications were necessary to obtain a closed-form solution. Especially good results are obtained for large μ (top plot) due to suppressed terms in the square-root of (37). Increasing N at fixed μ deteriorates the result to some extent as additional correction terms (the second order σ^{*2}-term) would be required to improve the result. The additional term, however, prevents a closed-form solution in terms of the W-function, see (38). Larger deviations occur for varying A, which is not surprising. Parameter A directly affects σ^*_{crit}, see Eq. (40) and Fig. 3, where for larger A one observes a significant decrease of σ^*_{crit} (larger extent of the progress dip). Furthermore, A is contained in the variance terms (14), which were mostly neglected. From the iteration shown in Fig. 4, one expects that the analytic solution should overestimate the numeric solution (see dip minima locations). Indeed, the analytic solution (magenta) lies consistently above the numeric solution in the bottom plot of Fig. 8. However, the overall scaling of approximation (40) w.r.t. A can be regarded as satisfactory. The polynomial solution (expanding Eq. (38) including terms $O(\sigma^{*2})$ and solving) significantly underestimates the expected results in all plots. Expanding the exponential function including $O(\sigma^{*4})$ did not improve the results, but gave mostly complex-valued solutions. This indicates that the exponential function is crucial to obtain acceptable results.

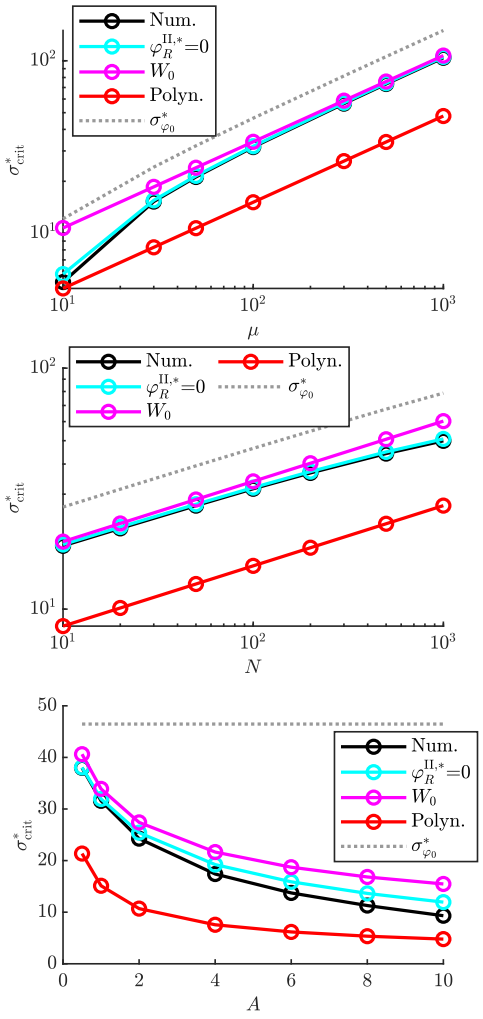

Fig. 8: Result for σ^*_{crit} evaluated for top ($N = 100$, $A = 1$, μ varied with $\vartheta = 0.5$), center ($\mu = 100$, $\lambda = 200$, $A = 1$, N varied), and bottom ($\mu = 100$, $\lambda = 200$, $N = 100$, A varied). The numeric evaluation using $\varphi_R^{\mathrm{II},*}(\sigma^*, R)$ (right plot of Fig. 4) is shown in black and serves as a reference. The cyan curve shows the numeric solution of $\varphi_R^{\mathrm{II},*}|_{R=R_\infty} = 0$ including all terms. The magenta curve shows result (40), and the red curve shows the solution of fourth order polynomial from (38) by expanding $\mathrm{e}^{-b\sigma^{*2}} = 1 - b\sigma^{*2} + O(\sigma^{*4})$. Note that the upper two plots use logarithmic axes.

E. Properties of $\tau(N, \alpha, A)$

Result (42) has important properties, which are discussed now. To this end, the substitution $x = \alpha\sqrt{A}/2$ is introduced, such that one has

$$\tau = \sqrt{\frac{1}{N}\left(1 - \frac{2}{x^2}W_0(x^3)\right)}. \tag{B.14}$$

Demanding $1 > \frac{2}{x^2}W_0\left(x^3\right)$ in (B.14) for a real-valued solution, one obtains by numeric solving

$$x_0 \approx 1.47, \quad \text{such that} \quad 1.47 < \frac{\alpha\sqrt{A}}{2}. \tag{B.15}$$

This condition is fulfilled for the standard (and larger) choices of α and A. Figure 9 shows $2W_0\left(x^3\right)/x^2$ as a function of x.

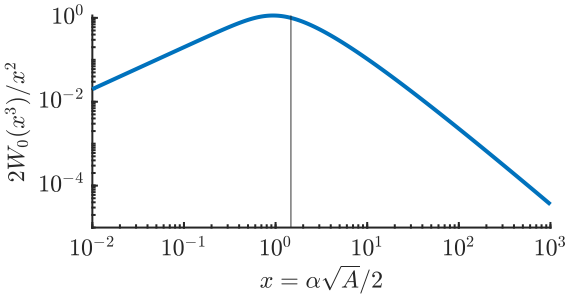

Fig. 9: W_0-dependence of τ from (B.14). The vertical line marks condition (B.15).

The vertical line indicates x above which there exists a real solution for τ. Note that the expression vanishes for large x. The limit $x \to \infty$ is evaluated now. An upper bound of $W_0(x)$ for $x \geq e$ is given by $W_0(x) \leq \ln(x) - \ln(\ln(x)) + \frac{e}{e-1}\frac{\ln(\ln(x))}{\ln(x)}$ [20], such that

$$\begin{aligned} W_0(x^3) &\leq \ln\left(x^3\right) - \ln\left(\ln\left(x^3\right)\right) + \frac{e}{e-1}\frac{\ln\left(\ln\left(x^3\right)\right)}{\ln(x^3)} \\ &= 3\ln(x) - \ln(3\ln(x)) + \frac{e}{e-1}\frac{\ln(3\ln(x))}{3\ln(x)}. \end{aligned} \tag{B.16}$$

The limit w.r.t. the upper bound vanishes as

$$\lim_{x\to\infty} \frac{2}{x^2}\left(3\ln(x) - \ln(3\ln(x)) + \frac{e}{e-1}\frac{\ln(3\ln(x))}{3\ln(x)}\right) = 0. \tag{B.17}$$

In the asymptotic limit $x \to \infty$, Eq. (B.14) therefore yields

$$\tau \simeq \sqrt{\frac{1}{N}}. \tag{B.18}$$

The limit $x \to 0$ is not useful from a modeling perspective, as for $\alpha\sqrt{A} \to 0$ the Rastrigin function becomes the sphere and σ^*_{crit} does not exists. Additionally, the residual distance R_∞ (36) vanishes for the sphere.

F. Additional Expected Runtime Experiment

For the experiment shown in Fig. 10, parameters $A = 1$, $\alpha = 2\pi$, and $N = 200$ were chosen. The varied strategy parameters are $\lambda = 100, 200, ..., 1000$, $\tau = 0.02, 0.03, ..., 0.08$, and $\vartheta = 0.1, 0.2, ..., 0.6$, resulting in 420 configurations. Each configuration is evaluated using 200 trials, such that P_S and E_r are obtained. An overall bugdet of function evaluations was set to $5 \cdot 10^6$. The legend is shown at the top with P_S on the left and $\log_{10}(E_r)$ on the right. The initialization was set to $\mathbf{y}^{(0)} = 3 \cdot \mathbf{1}$, $\sigma^{(0)} = \sigma^*_{\varphi_0}\|\mathbf{y}\|/N$ and the termination criteria are the same as in Sec. VI.

The overall results are comparable to the experiment in Sec. VI. The lowest E_r is obtained for moderate $\tau \approx 0.5$, which agrees well with Eq. (42) giving $\tau(N, \alpha, A) \approx 0.0495$. The default $\tau = 1/\sqrt{2N} = 0.05$ is also very close to $\tau(N, \alpha, A)$ for this configuration. Large values of τ tend to be more unstable, while small values are less efficient. Again, the highest success rates are obtained for larger ϑ and small τ, which is not surprising. Furthermore, sphere-optimal truncation ratios around $\vartheta = 0.25$ tend to be more efficient.

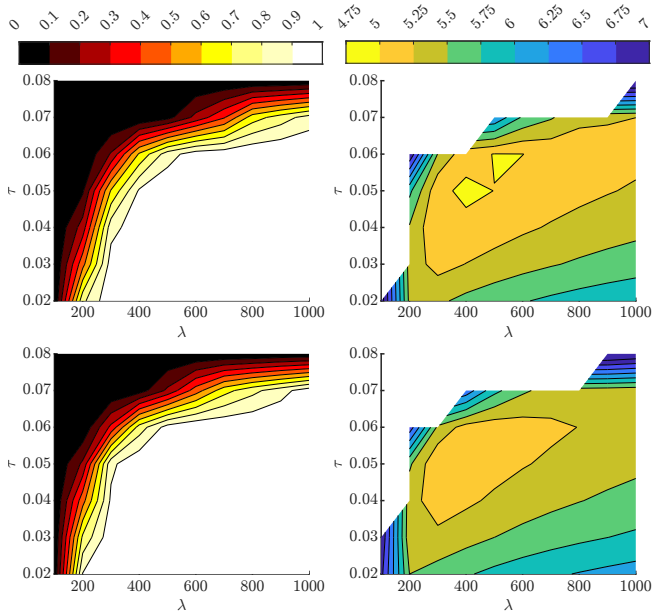

(a) Variation of λ (x-axis) and τ (y-axis) for $\vartheta = 0.3$ (top) and $\vartheta = 0.5$ (bottom).

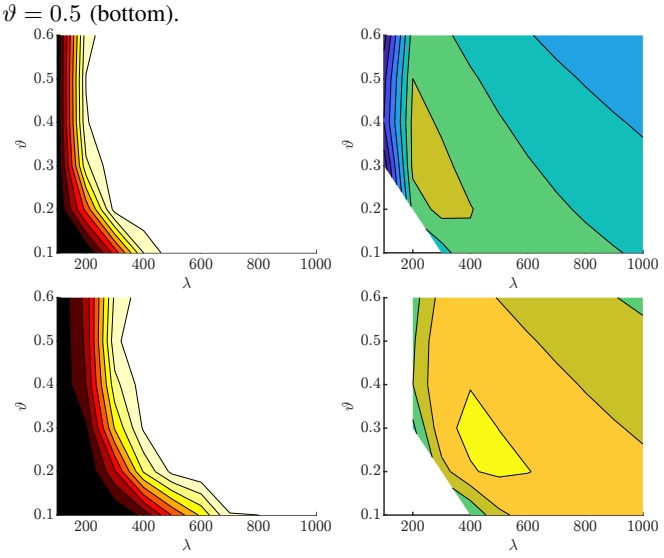

(b) Variation of λ (x-axis) and ϑ (y-axis) for $\tau = 0.02$ (top) and $\tau = 0.05$ (bottom).

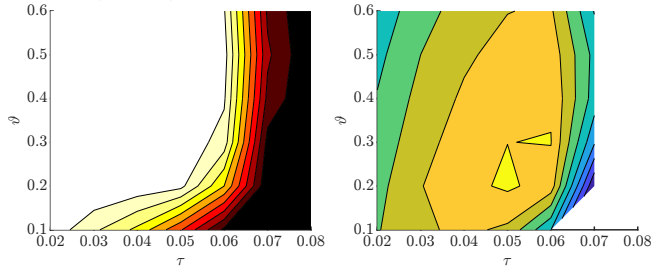

(c) Variation of τ (x-axis) and ϑ (y-axis) for $\lambda = 500$.

Fig. 10: Variation of λ, τ, and ϑ at $A = 1$ and $N = 200$. The left column shows the success rate P_S. The right column shows $\log_{10}(E_r)$, see (43). The legend is placed at the top.